water

MDPI

Article

The Seasonal Dynamics of Organic and Inorganic Carbon along the Tropical Usumacinta River Basin (Mexico)

Ismael Soria-Reinoso [1], Javier Alcocer [2,*], Salvador Sánchez-Carrillo [3], Felipe García-Oliva [4], Daniel Cuevas-Lara [1], Daniela Cortés-Guzmán [1] and Luis A. Oseguera [2]

1 Posgrado en Ciencias del Mar y Limnología, Universidad Nacional Autónoma de México, Av. Universidad 3000, Alcaldía Coyoacán, C. P., Mexico City 04510, Mexico
2 Grupo de Investigación en Limnología Tropical, FES Iztacala, Universidad Nacional Autónoma de México, Av. De los Barrios N° 1, Los Reyes Iztacala, Tlalnepantla 54090, Mexico
3 Departamento de Biogeoquímica y Ecología Microbiana, Museo Nacional de Ciencias Naturales (CSIC), Serrano 115 dpdo, 28006 Madrid, Spain
4 Instituto de Investigaciones en Ecosistemas y Sustentabilidad, Universidad Nacional Autónoma de México, AP 27-3, Santa María de Guido, Morelia 58090, Mexico
* Correspondence: jalcocer@unam.mx; Tel.: +52-55-5623-1333 (ext. 39719)

Abstract: Rivers are important sites for carbon (C) transport and critical components of the global C cycle that is currently not well constrained. However, little is known about C species' longitudinal and temporal changes in large tropical rivers. The Usumacinta River is Mexico's main lotic system and the tenth largest in North America. Being a tropical river, it has a strong climatic seasonality. This study aims to evaluate how organic (DOC and POC) and inorganic (DIC and PIC) carbon change spatially and seasonally along the Usumacinta River (medium and lower basin) in rainy (RS-2017) and dry (DS-2018) seasons and to estimate C fluxes into the southern Gulf of Mexico. Concentrations of DOC, POC, DIC, and PIC ranged from 0.88 to 7.11 mg L^{-1}, 0.21 to 3.78 mg L^{-1}, 15.59 to 48.27 mg L^{-1}, and 0.05 to 1.51 mg L^{-1}, respectively. DOC was the dominant organic species (DOC/POC > 1). It was ~doubled in RS and showed a longitudinal increase, probably through exchange with wetlands and floodplains. Particulate carbon showed a positive relationship with the total suspended solids, suggesting that in RS, it derived from surface erosion and runoff in the watershed. DIC is reported for the first time as the highest concentration measured in tropical rivers in America. It was higher in the dry season without a longitudinal trend. The C mass inflow–outflow balance in the RS suggested net retention (DOC and POC sink) in floodplains. In contrast, in the DS, the balance suggested that floodplains supply (C source) autochthonous DOC and POC. The lower Usumacinta River basin is a sink for DIC in both seasons. Finally, the estimated annual C export for the Usumacinta-Grijalva River was 2.88 (2.65 to 3.14) Tg yr^{-1}, of which DIC was the largest transported fraction (85%), followed by DOC (10%), POC (4%), and PIC (<1%). This investigation is the first to present the C loads in a Mexican river.

Keywords: carbon biogeochemistry; dissolved organic carbon; dissolved inorganic carbon; particulate organic carbon; Centla wetlands; tropical river; Usumacinta-Grijalva Rivers

Citation: Soria-Reinoso, I.; Alcocer, J.; Sánchez-Carrillo, S.; García-Oliva, F.; Cuevas-Lara, D.; Cortés-Guzmán, D.; Oseguera, L.A. The Seasonal Dynamics of Organic and Inorganic Carbon along the Tropical Usumacinta River Basin (Mexico). *Water* **2022**, *14*, 2703. https://doi.org/10.3390/w14172703

Academic Editors: Yijun Xu and Siyue Li

Received: 30 June 2022
Accepted: 26 August 2022
Published: 30 August 2022

1. Introduction

Inland waters cover only a tiny fraction (about 1%) of the Earth's surface [1] but play disproportionate roles in the global carbon (C) cycle [2–4]. Rivers are functional interfaces for the transport, processing, and exchange of C between terrestrial ecosystems [5–7]; the atmosphere [8,9]; and the marine environment [10–12] throughout the aquatic continuum [13–15]. Over the last decade, the annual rate of C transported by rivers globally to the oceans (1.06 Pg C yr^{-1}; 1 Pg = 10^{15} g) [16] is on the same order of magnitude as the rate of C sequestration by land (3.4 ± 0.9 Pg C y^{-1}) or than the oceanic uptake of atmospheric CO_2 (2.5 ± 0.6 Pg C yr^{-1}) [17]. The total annual C exported by worldwide rivers includes

0.41 Pg of dissolved inorganic C (DIC), 0.24 Pg of dissolved organic C (DOC), 0.24 Pg of particulate organic C (POC), and 0.17 Pg of particulate inorganic C (PIC) [16].

Riverine C originates from natural and anthropogenic sources; however, anthropogenic influences are complex and difficult to quantify [5]. The lateral transport of terrestrial net PP (plant and litter detritus or leached material) and the export of terrestrial inorganic C (chemical weathering of silicate and carbonate minerals and soil respiration, as well as erosion of carbonate rocks) are the principal pathways through which C enters the fluvial systems [5]. However, the biogeochemical processes involved in river C fluxes are still unclear because physical and biological factors vary widely along the hydrological continuum [14,15].

Inputs of organic C (OC) alter the metabolism of both river and connected downstream water bodies and are vital for sustaining coastal heterotrophy [18]. Both DOC and POC play significant roles in the river C cycle. However, DOC is the primary energy source sustaining the heterotrophic aquatic metabolism, resulting in a large amount of CO_2 outgassing to the atmosphere [19]. Riverine DOC results from the balance between both allochthonous terrestrial (leaching of dissolved organic matter -OM- from soils through runoff) and autochthonous (derived from fluvial productivity -PP-) contributions and microbial consumption, flocculation, and photodegradation processes [19,20]. DOC fluxes are determined by several factors (e.g., hydrological events, basin slope, soil C), showing considerable spatial and seasonal variation within a catchment [16,20], with higher values in wetlands and around rainfall events [21,22]. Otherwise, POC originates from fresh leaf litter, PP, and wastewater discharges and the weathering and oxidation of OC contained in sedimentary rocks (or petrogenic OC [12,23]). DOC/POC ratios vary widely between rivers, from 10:1 in temperate forests to 1:1 in grassland areas [24]. In low-relief tropical basins with wetland presence, the DOC/POC ratio is >1 [25]. In contrast, in humid regions with mountainous relief, such as the Asian monsoon basins or the upper Amazon River basin, the DOC/POC ratio is <1 [12]. As a result of gravitational settling, hydrodynamic lift, and drag forces [19], a strong correlation between POC concentration, total suspended solids (TSS), and discharge has been found for most worldwide river systems [12,26].

Over geologic time, rivers have transported C due to the chemical weathering of carbonate and silicate rocks to storage in marine sinks [27,28]. DIC is the most significant part of river C entering the oceans [11,26] and consists of bicarbonate (HCO_3^-) and carbonate (CO_3^{2-}) as well as CO_2 dissolved in riverine water, with the chemical equilibrium depending on temperature and pH [29]. When river water pH oscillates from 6 to 8.5, HCO_3^- is the dominant component, the most usual form in which DIC appears [20,30]. DIC concentration is controlled by: (i) the lithology and the weathering of carbonate/silicate rocks, (ii) the soil CO_2 released by the terrestrial OM decomposition and transported to the river, (iii) the exchange of CO_2 at the water–air interface, and (iv) the internal river processes that release CO_2 through the decomposition of allochthonous and autochthonous OM and trigger the C uptake by the PP [31–33]. Carbonated river basins display a DIC concentration an order of magnitude greater than that of non-carbonated crystalline basins (volcanic or plutonic rocks) [12]. PIC originates from the mechanical erosion of carbonate rocks (limestone, slate). However, it can be dissolved as DIC downstream [34] or gradually precipitate, trapped in floodplains and estuaries before reaching the coastal waters [35]. Despite its significant effect on DIC, PIC usually does not account for the overall C budget because it is considered a transfer of carbonate minerals from the river headwaters to the oceans [11].

Tropical regions account for 42.7% of global area, but they contribute the highest percentage of freshwater (~66%), sediment (~73%), and C (~50%) discharging to the worldwide oceans [11,16]. Tropical rivers are hotspots of C export to the sea, displaying a high hydrological seasonality according to rainy and dry seasons [36,37]. Nevertheless, magnitude and C processing have been poorly studied in tropical rivers despite their disproportionate importance compared with rivers from other latitudes [15]. During the past decade,

research on C in low-latitude areas has been strongly encouraged in America [23,38–44], Africa [45–51], and Asia [52–57], but it is not enough yet.

In tropical America, a lack of knowledge about the role of river systems in the regional C cycle is evident [58–60]. Mexico has the largest rivers in Central America, but scientific knowledge of these rivers is still incipient. The Usumacinta River is Mexico's most important lotic system and the tenth largest in North America [61,62]. It drains into the southern Gulf of Mexico under a tropical seasonality defined by a rainy season in summer and a dry season in winter [63]. It is assumed that the Usumacinta River plays an essential role in the regional C balance, particularly in DIC fluxes to the Gulf of Mexico, due to carbonaceous lithology [61]. However, this has been poorly studied compared with other South American [41,64,65] and North American rivers [66–68]. A recent study [42] on the POC dynamics in the Usumacinta River revealed a strong seasonality in sources, concentrations, and fluxes. Furthermore, during the dry season, the wetlands of the lower basin function as a POC source, while in the rainy season, they are a sink for POC, mainly allochthonous [42]. Nevertheless, the spatial and temporal variation of dissolved C and the role of floodplains on the retention or delivery of DOC, DIC, and POC to the mainstem are still unknown. The present study is an effort to fill this gap in our knowledge.

This research aims to generate baseline information on the seasonal and spatial changes in the C concentration and fluxes in the Usumacinta River basin, along with the river's hydrochemistry parameters. This work pursued evaluating the longitudinal pattern of C concentrations and fluxes in the middle and lower basin of the Usumacinta River to identify the variability in C fractions according to tropical climatic seasonality (rainy vs. dry season) and to estimate the C fluxes and quantify the C discharged to the southern Gulf of Mexico. Since this investigation was exploratory in nature, it tested no hypothesis. However, based on the basin's dominant carbonaceous lithology and its tropical location, we expected DIC to be the dominant C fraction and that large changes in C concentration and fluxes would mirror the strong seasonality.

2. Materials and Methods

2.1. The Usumacinta River

This study was carried out in the Mexican portion (medium and lower basin) of the Usumacinta River, southeast Mexico. The Usumacinta River is part of the Usumacinta-Grijalva Hydrological Region 30 (HR-30), which is Mexico's most extensive river system [62] and the tenth largest in North America [61]. HR-30 is the largest discharge in Mexico and the second-largest overall to the Gulf of Mexico after the Mississippi River [69]. The drainage basin is ~112,550 km^2, and the flow range is between 3000 and 6000 $m^3\ s^{-1}$, equivalent to around 30% of the total surface runoff of Mexico [63,70]. The Usumacinta River basin extends over Guatemala (58% of the total area) and Mexico (42%). It covers an area of 77,743.6 km^2 between longitudes 89–92° W and latitudes 14–18° N [61]. The Usumacinta is the largest river in Mesoamerica (~1100 km). It originates in the Sierra de Los Cuchumatanes Mountain range in Guatemala (3800 m a.s.l), then enters Mexican territory through the Lacandona rainforest and flows through the Mexican states of Chiapas and Tabasco. The Grijalva River, in a parallel contiguous basin, artificially joins the Usumacinta River 15 km before the river's mouth at the southern Gulf of Mexico [71], forming a large (20,000 km^2) freshwater wetland known as Pantanos de Centla Biosphere Reserve [61,69]. The mainstem remains unimpounded and is fed by the waters released from the following catchments: the Chixoy-Salinas (13,643 km^2), La Pasión (11,795 km^2), Lacantún (19,980 km^2), and San Pedro rivers (13,964 km^2) [69].

The climate in the region is tropical humid, characterized by a tropical monsoon rainfall schedule set up by a rainy season (June to November; RS; ~2500 mm yr^{-1}) in summer and a dry season (December to May; DS; ~800 mm yr^{-1}) in winter [72,73]. Moreover, heavy rains and windy episodes called *nortes* occur between October and March [71,74]. The climate is controlled by the Intertropical Convergence Zone (ITCZ) and El Niño/La Niña events that affect the Atlantic and Pacific Ocean surface temperatures [73,75]. In some areas of

the highlands, the rainfall reaches up to 6000 mm, considered one of the highest levels in Mexico and Mesoamerica [71]. The average annual temperature (~23 °C) varies from 8–12 °C in the Altos Cuchumatanes (Guatemala) up to 29–32 °C in the lower basin [61]. The only gauging station in the Usumacinta River basin is at Boca del Cerro (Figure 1; M10). It covers a drainage area of 47,697 km^2 [76,77] with an average annual flow rate of 2085 m^3 s^{-1} [78].

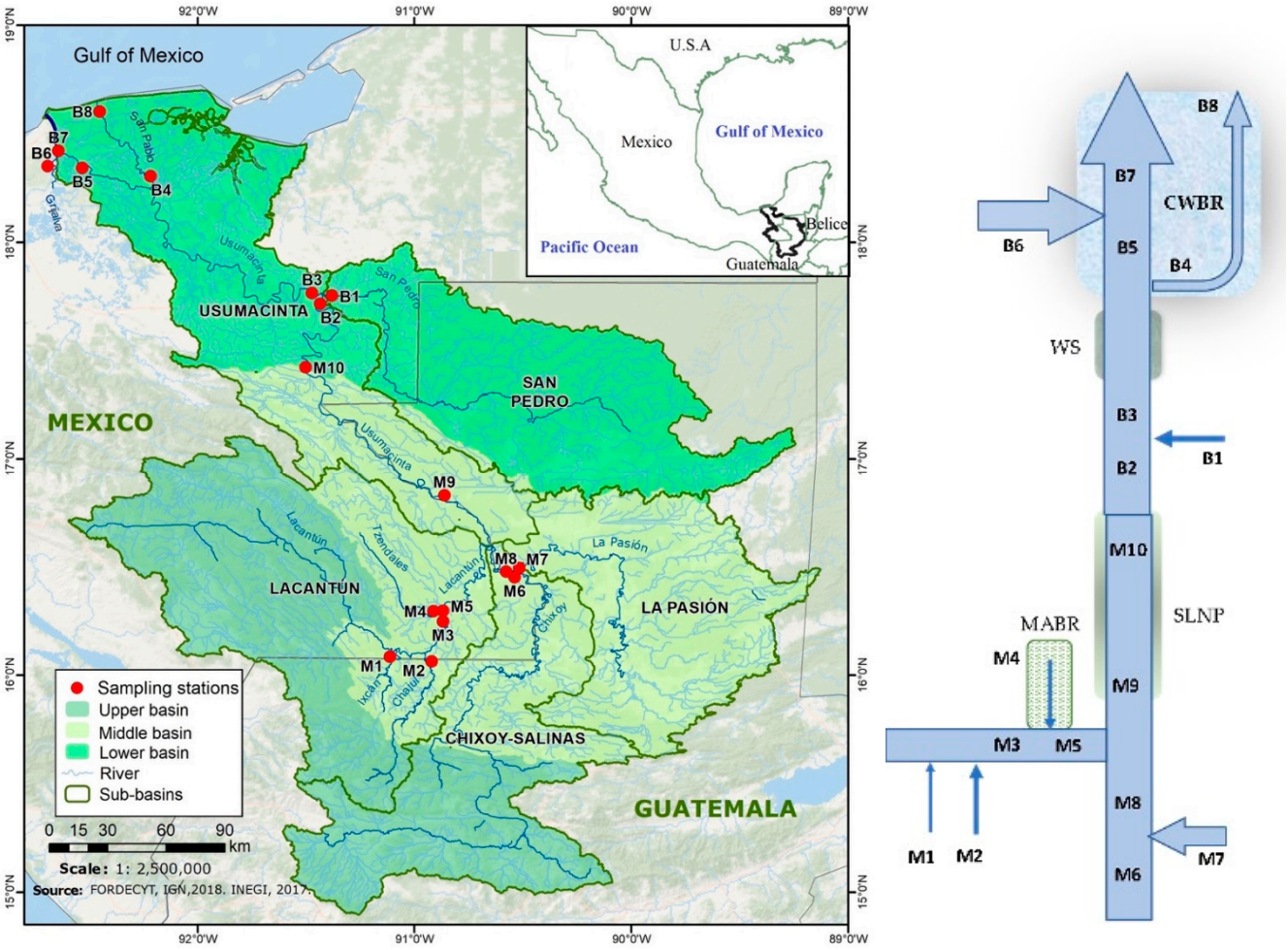

Figure 1. Map (**left**) and diagram (**right**) of the Usumacinta River basin indicating the sampling stations. (M = middle basin and B = lower basin stations). MABR = Montes Azules Biosphere Reserve; SLNP = Sierra de Lacandon National Park; WS = wetland system; CWBR = Pantanos de Centla Biosphere Reserve.

The vegetation in the middle basin is mainly composed of tropical and subtropical forests [61]. Recently, the evergreen, coniferous, and oak forests that covered ~85% of the middle basin have been reduced due to agricultural activities and extensive livestock [79]. The lower basin is integrated with mangrove swamps, marshes, and hydrophytic vegetation [80,81]. The mountainous area (middle) and the coastal plain (lower) are the main distinctive geomorphological units along the Usumacinta River basin [82]. The mountainous region is composed of the Sierra de Los Cuchumatanes-Guatemala (extensive folded block of Cretaceous limestone and dolomites), the Sierra Madre de Chiapas-Mexico (diorites and granites from the Paleozoic), and the Altos de Chiapas (marine and continental carbonates from the Mesozoic with volcanic deposits from the Cenozoic). The Coastal Plain is a low-relief area (slope from 0 to 3%) where the river delta develops through diverse freshwater and coastal wetlands. The landscape geology is dominated by sedimentary Cenozoic rocks of alluvial and lacustrine origin [71,83,84]. According to Olea [85], the domi-

nant chemical water type in the Usumacinta River is Ca-Mg-SO_4-HCO_3 in the dry season and Ca-Mg-HCO_3-SO_4 in the rainy season.

2.2. Sampling

Two sampling campaigns were carried out, during the 2017 rainy season (October) and the 2018 dry season (April), at 18 sampling sites covering the middle (M1 to M10) and lower (B1 to B8) Usumacinta River basins, including the main tributaries. Sampling sites were the Ixcán (M1) and Chajul (M2) rivers that originate in Guatemala and drain toward the Lacantún River (M3), which receives the waters of the Tzendales River (M4). This site is in the central part of the Montes Azules Biosphere Reserve (MABR, a protected area within the Lacandona Forest). Additionally, sampling was conducted of the Lacantún (M5), Chixoy (M6), La Pasión (M7), San Pedro (B1), and Grijalva (B6) rivers, as well in the mainstem of the Usumacinta River (M8, M9, M10, B2, B3, B5, B7). Finally, the San Pedro-San Pablo River (B4 and B8) was sampled at the lower basin, accounting for the smaller river mouth of the Usumacinta River (Table S1; Figure 1).

A river cross-section was recorded at each site using a Garmin echo-sounder (model GPSMap 526S Sounder). Then, three vertical profiles along the sampling section (one center point and two more equidistant from both sides) were compiled, measuring water temperature, dissolved oxygen (DO), pH, electrical conductivity at 25 °C (K_{25}), turbidity, and oxidation/reduction potential (ORP) using a Hydrolab DS5 Multiparameter sonde equipped with a data logger (Surveyor 4a). The DS5 probe recorded a vertical profile from the surface to the maximum depth with a vertical resolution of one meter. The nominal precisions were as follows: temperature ±0.10 °C; DO ±0.2 mg L^{-1}; pH ±0.2; K_{25} ±0.001 mS cm^{-1}; turbidity ±1 NTU and ORP ±20 mV. Water flow was measured at each site using a Swoffer 3000 current meter (1% accuracy). Five successive speed measurements were made of each vertical profile at 1/3 of the maximum depth to obtain a mean representative value. Water samples were taken from each vertical profile at 1/3 of the maximum depth for each sampling station, using a horizontal Van Dorn bottle [42]. The water samples were filtered in situ, and the filters were transported in dark and cold conditions until they were analyzed at FES Iztacala Laboratory–UNAM for total suspended solids (TSS) and chlorophyll-a (Chl-a) and at the Center for Marine Science at UNC Wilmington (for DOC, POC, DIC).

2.3. Analytical Methods

Water samples for TSS, POC, and total particulate carbon (TPC) analysis were first passed through a 100 µm mesh to remove large particles. Two replicates of each vertical water profile were filtered (TSS: 200 to 2000 mL; POC and TPC: 20 to 100 mL) with a vacuum pump (0.3 to 0.5 atm) through pre-combusted (550 °C, four hours) Whatman GF/F filters (TSS: 47 mm diameter, pore size: 0.7 µm; POC and TPC: 13 mm, 0.7 µm). TSS concentrations were obtained gravimetrically after filter desiccation (60 °C, 24 h) with a Mass Comparator Balance (Mettler Toledo). The precision of the weight measurements was 0.1 mg. POC filters were first acidified using 10% HCl to remove carbonates before analysis and then oven-dried (50 °C, 24 h). Subsequently, the dried filters were packed in aluminum foil for analysis on a CHN analyzer Carlo Erba NC2100. This procedure was similar for measuring TPC, but the filters were not acidified after filtration. The difference between the POC and TPC concentrations was assumed to be the concentration of particulate inorganic carbon (PIC) [42].

For the DOC analysis, samples for each vertical profile were filtered in duplicate through a GF/F (0.7 µm nominal pore size) filter previously combusted (550 °C, four hours) and stored in 40 mL amber glass vials with polytetrafluoroethylene (PTFE)-coated septa. The filtered sample was acidified with H_3PO_4 (40%) to make the pH < 2 for the removal of DIC. DOC concentrations were analyzed with high-temperature combustion using a Shimadzu TOC 5000 total organic carbon analyzer equipped with an ASI 5000

autosampler. We also calculated the total organic carbon (TOC) as the sum of the dissolved and particulate OC in each vertical profile.

Water samples for the DIC in each vertical profile were filtered in duplicate (GF/F; 0.7 μm) and recovered in 60 mL (BOD Wheaton) borosilicate glass bottles at once; then, 25 μL of saturated (50%) aqueous mercuric chloride ($HgCl_2$) solution was added to inhibit any biological activity. Bottles were filled (without any air left) to avoid exchanges with ambient air CO_2 and sealed with grease on the ground glass stopper. A rubber band on the stopper was then secured with tape. DIC concentrations were analyzed in a Shimadzu TOC 5000 Analyzer.

Triplicate water samples (20 to 100 mL) for each vertical profile were filtered (Whatman 0.7 μm GF/F) for Chl-a analysis. The pigments were extracted with 10 mL acetone (90%) at 4 °C overnight. Chl-a was analyzed in a Turner Designs TD. 10-AU fluorometer (EPA method 445.0) [86].

2.4. Data Analysis and Statistical Methods

The water discharge ($m^3\ s^{-1}$) was calculated using the area–velocity method. Instantaneous C fluxes of each fraction (DOC, POC, TOC, DIC, PIC) were obtained by multiplying the measured water discharges by the corresponding C fraction concentration at each station (t d^{-1}). The total carbon (TC) was calculated as the sum of the dissolved and particulate chemical species (TC = DOC + POC + DIC + PIC).

The mass inflow–outflow balance of C fractions in the lower basin was calculated according to [68,87]. We calculated the difference between the last site of the middle basin (M10, input) and the two Usumacinta River mouths (B5 and B8, output) at the lower basin (Figure 1). We chose these sampling points because B5 represents the mainstem before its merge with the Grijalva River (B6), and B8 is the freshwater end-member in the second mouth after crossing the Pantanos de Centla Biosphere Reserve, as mentioned by Cuevas-Lara [42]. Thus, the difference (M10 − (B5 + B8)) determines whether the lower basin river stretch was either a C retention area (sink, M10 − (B5 + B8) > 0) or a source area (M10 − (B5 + B8) < 0) for the different C fractions. However, this C balance does not recognize the involved C processes, transformations, or fate, such as CO_2 evasion or C storage in floodplains or sediments (including outgassing to the atmosphere in the case of DIC) [87]. Similarly, the flux difference was also expressed as a percentage of the upstream change at Boca del Cerro (M10).

Averages, standard deviations, and ranges were calculated for each variable. We computed the distance to the river mouth (Table S1) with a map projection using the WGS84 data. All variables were plotted for distance to the mouth to define longitudinal trends. ANOVA (Shapiro–Wilk normality test passed) and the nonparametric Kruskal–Wallis ANOVA (normality test failed) were used to assess significant differences in seasonal variability among the physicochemical variables, C concentrations, and fluxes. The nonparametric Spearman rank-order correlations were used to evaluate relationships between C concentrations and environmental variables in the RS and the DS of the Usumacinta River. All statistical analyses were performed using Sigmaplot v14.0, and an α level of 0.05 was used to determine significance.

2.5. Annual Flux Calculation

Excepting POC [42], no data are available on C transport in the Usumacinta River; therefore, we used our database for a rough estimate of the annual dissolved and particulate C discharge following the proposed method by [50] for the Senegal River, West Africa. We used the daily flows from Banco Nacional de Datos de Aguas Superficiales (BANDAS) [76] of the Boca del Cerro gauging station (M10) corresponding to our study period between July 2017 and July 2018. Additionally, the C concentration (average, minimum, and maximum) was measured in M10 in the RS and DS. The daily Q from June to December (high flow period) was multiplied by the C concentration of the RS. Meanwhile, the daily Q from January to May (low flow period) was multiplied by the C concentration of the DS [50].

However, due to the high flow recorded in February 2018 (see Section 3.1), the annual average (2456 m^3 s^{-1}) was considered the limit for the calculation. That is, daily flow values higher than the average were used within the RS and lower in the DS. Daily flows were summed and expressed in Tg yr^{-1}. However, the Boca del Cerro (M10) gauging station has a distance to the mouth of ~385 km, and the channel flows through a wetland and floodplain system in the lower basin that reduces Q (see Figure S1) and modifies C loads (see Sections 3.2 and 3.4). In addition, the Grijalva River (B6) influences the final discharge. For these reasons, a re-estimation of the C flux was performed considering the sampling stations at the mouth (B7 + B8). We also calculated the C yields using (t C km^2 yr^{-1}) Q × C concentration/watershed area for the entire Usumacinta-Grijalva River basin. While this approach is widely used in flux calculation for large rivers, inevitable error exists in the estimation, mainly due to the large variability of discharge across the year.

3. Results

3.1. Discharge and Physical and Chemical Variables of the Usumacinta River

The Usumacinta River showed significant temporal variations in its environmental variables. Tables S2 and S3 show the average values of the physical and chemical parameters measured at the 18 sampling sites in the middle and lower basins of the Usumacinta River. Most parameters changed significantly over the two seasons.

The Q was approximately 6 times higher during the RS (from 141 m^3 s^{-1} to 5970 m^3 s^{-1}) than in the DS (from 15 m^3 s^{-1} to 1080 m^3 s^{-1}), with significant differences between sampling campaigns (H = 9.42; p = 0.002). Q in the mainstem evidenced an increasing trend in the middle basin and a decrease toward the mouth (Figure S1). Comparing the Q of Boca del Cerro (M10) with the mainstem of the lower basin and San Pedro-San Pablo (B5 + B8), the Q decreased ~49% in the RS and ~18% in the DS (Tables S2 and S3). However, the Grijalva River (B6) inflow increased Q (50% in the RS and 35% in the DS; Figure S1). The final discharge (B7 + B8) from the Usumacinta River to the Gulf of Mexico was five times greater in the rainy (5748 m^3 s^{-1}) than in dry seasons (1194 m^3 s^{-1}).

Based on the gauging data recorded at Boca del Cerro (M10) [76], we constructed the hydrograph from July 2017 to July 2018 (Figure 2). The average flow for this period was 2456 m^3 s^{-1} and ranged from 678 m^3 s^{-1} (8 May 2018) to 6722 m^3 s^{-1} (30 October 2017). The discharge in the RS (5970 m^3 s^{-1}) doubled the historical average for the rainy season (~2851 m^3 s^{-1}). The flow at DS (998 m^3 s^{-1}) was ~1.5 times higher than the historical Q for this season (~678 m^3 s^{-1}).

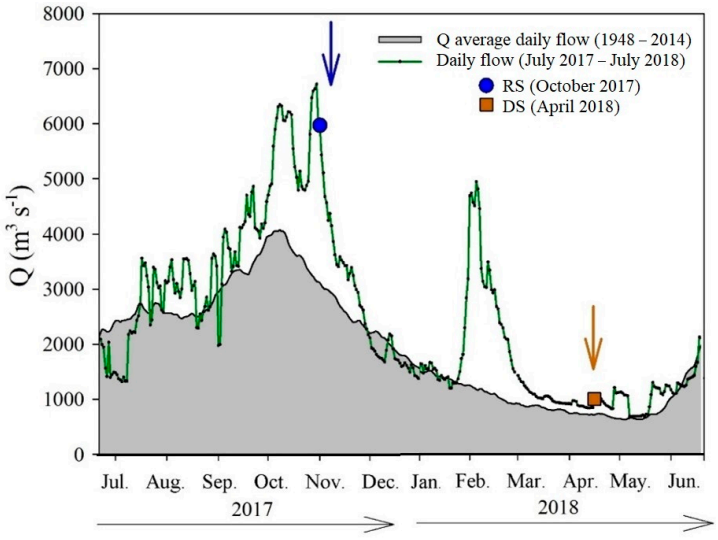

Figure 2. Variations in the historical (1948–2014) average daily flow (grey area) and the 2017 (RS) to 2018 (DS) flow measured at the hydrometric station at Boca del Cerro (M10), Tabasco.

Average water temperature (H = 20.5, $p < 0.001$), DO (H = 10.4, p = 0.001), pH (F = 12.7, p = 0.001), and electrical conductivity (H = 20.8, $p < 0.001$) were higher in the DS than in the RS (Tables S2 and S3). Meanwhile, ORP (H = 37.3, $p < 0.001$), and TSS (H = 17.2, $p < 0.001$) concentrations were higher in the RS. Similarly, all sampling stations had significantly higher turbidity in the RS than the DS, except B3 (Usumacinta and San Pedro confluence; U = 1213, p = 0.112) and B8 (San Pedro-San Pablo; U = 433, p = 0.260). Chlorophyll-*a* concentration was higher in the DS ($p < 0.05$) in all sampling sites, except in Lacantún (M3; p = 0.5), Chixoy (M6; p = 0.5), and the Usumacinta-Grijalva confluence (B7; p = 0.29).

High water temperatures (mean 26.5 ± 2.3 °C) prevailed in both sampling campaigns, ranging between 20.8 °C (M1, RS) and 29.8 °C (M7, DS). The DO of the Usumacinta River ranged from 1.4 mg L^{-1} (B6, RS) to 10.8 mg L^{-1} (M1, DS), with a mean of 6.8 ± 2.4 mg L^{-1}. The pH was slightly alkaline, from 7.3 (M7, RS) to 8.3 (M2, DS) with an average of 7.8 ± 0.3. Overall, the Usumacinta River behaved as an oxidizing environment (349 ± 43 mV) and ranged from 226 mV (M4, DS) to 428 mV (M10, RS). Electrical conductivity (K_{25}) ranged from 241 µS cm^{-1} (M2, RS) to 37,144 µS cm^{-1} (B8, DS) with an average of 375 ± 109 µS cm^{-1} in the RS and 6117 ± 11,325 µS cm^{-1} in the DS. K_{25} showed behavior associated with seawater intrusion in the closest stations to the river's mouths and only in the DS. In the RS, K_{25} did not exceed 1000 µS cm^{-1} at any site.

The turbidity measurements show a wide range, between 5 NTU (B1, RS) and 102 NTU (M1, RS) and averaging 48 ± 23 NTU. The Usumacinta River TSS concentration (42.4 ± 36.6 mg L^{-1}) ranged from 3.2 mg L^{-1} (M4, DS) to 119.0 mg L^{-1} (M3, RS). The concentration of TSS in the mainstem decreases downstream in both seasons (Tables S2 and S3).

Chlorophyll-a concentrations ranged between 0.12 µg L^{-1} (M4; RS) and 13.4 µg L^{-1} (B8, DS), with a mean of 1.8 ± 1.40 µg L^{-1} in the RS and 3.24 ± 3.30 µg L^{-1} in the DS. There was a significant Chl-a concentration increasing trend following the distance to the river mouth in both seasons (Tables S2 and S3, and Figure S2).

3.2. Temporal and Spatial Variation of Carbon Concentration

Table 1 shows the average concentrations of DOC, POC, TOC, DIC, and PIC measured at the 18 sampling sites in the middle and lower basins of the Usumacinta River.

Table 1. Carbon concentrations at the Usumacinta River sampling stations during the rainy (RS) and dry seasons (DS). (For all variables, the average is in the first grey row, and the standard deviation is in the second, "-" indicates no data).

Code	DOC (mg L^{-1})		POC (mg L^{-1})		TOC (mg L^{-1})		DIC (mg L^{-1})		PIC (mg L^{-1})	
	RS	DS	RS	DS	RS	DS	RS	DS	RS	DS
M1	1.10	0.88	1.74	0.35	2.85	1.23	23.69	26.84	1.42	0.05
	0.01	0.02	0.38	0.05	0.36	0.07	0.23	1.26	0.18	0.04
M2	1.34	1.44	2.02	0.21	3.36	1.64	22.91	15.59	1.51	0.12
	0.34	0.49	0.63	0.01	0.29	0.48	0.11	0.15	0.38	0.10
M3	1.54	1.30	3.78	0.36	5.32	1.66	34.25	31.64	1.38	0.09
	0.60	0.10	0.73	0.08	0.78	0.07	0.99	0.21	0.53	0.04
M4	1.39	1.00	1.27	0.30	2.67	1.30	47.19	35.19	0.27	0.08
	0.07	0.18	0.06	0.02	0.07	0.15	0.17	2.85	0.19	0.01
M5	1.98	0.96	2.32	0.27	4.30	1.23	31.41	31.38	1.42	0.07
	0.06	0.11	0.73	0.02	0.64	0.06	5.82	0.56	0.27	0.01
M6	2.72	1.82	1.27	0.97	3.96	2.79	23.38	23.83	1.17	0.24
	0.15	0.22	0.26	0.17	0.34	0.16	1.54	3.25	0.25	0.09
M7	4.68	1.50	0.44	0.36	5.12	1.87	31.13	48.27	0.09	0.06
	0.22	0.21	0.05	0.05	0.11	0.13	2.47	0.29	0.06	0.03
M8	3.72	1.66	1.02	0.79	4.74	2.44	28.63	36.11	0.71	0.18
	0.49	0.23	0.09	0.17	0.42	0.16	0.94	1.51	0.35	0.14
M9	2.78	1.82	1.07	0.89	3.86	2.71	28.34	28.76	0.25	0.17
	0.26	0.51	0.15	0.09	0.17	0.50	0.93	1.67	0.10	0.10

Table 1. *Cont.*

Code	DOC (mg L^{-1})		POC (mg L^{-1})		TOC (mg L^{-1})		DIC (mg L^{-1})		PIC (mg L^{-1})	
	RS	DS	RS	DS	RS	DS	RS	DS	RS	DS
M10	3.00	1.45	0.96	0.61	3.97	2.06	31.16	37.58	0.48	0.26
	0.13	0.32	0.05	0.03	0.19	0.22	0.28	1.31	0.42	0.10
B1	7.11	3.26	0.64	0.75	7.75	4.02	29.91	37.44	0.11	-
	0.32	0.40	0.04	0.02	0.29	0.38	0.44	0.50	0.03	-
B2	3.02	1.60	1.09	0.93	4.14	2.53	30.16	38.58	0.48	0.14
	0.16	0.08	0.42	0.12	0.35	0.22	0.95	0.05	0.16	0.15
B3	3.18	1.87	0.81	0.85	4.04	2.71	30.59	39.96	0.38	0.16
	0.59	0.41	0.17	0.08	0.62	0.30	0.14	0.71	0.31	0.07
B4	3.73	1.94	1.40	1.18	5.13	3.12	30.80	35.61	0.32	0.40
	0.06	0.12	0.02	0.26	0.08	0.14	0.0	1.51	0.09	0.08
B5	3.30	1.62	1.62	0.79	4.92	2.41	29.86	34.52	0.27	0.26
	0.26	0.30	0.54	0.18	0.41	0.14	0.26	3.37	0.30	0.10
B6	5.23	2.02	2.42	0.60	7.65	2.63	29.04	31.74	0.37	0.22
	0.35	0.29	0.44	0.07	0.43	0.30	1.07	0.06	0.10	0.05
B7	4.73	1.62	2.57	0.52	7.30	2.15	29.17	31.27	0.53	0.10
	0.70	0.22	1.00	0.09	1.70	0.19	0.19	2.26	0.29	0.05
B8	6.90	2.86	2.24	1.45	9.14	4.31	30.50	31.61	0.82	0.21
	0.87	0.52	0.46	0.16	0.50	0.19	0.13	1.55	0.41	0.01
Average	3.42	1.70	1.59	0.68	5.01	2.38	30.12	33.11	0.67	0.17
SD	1.77	0.60	0.84	0.34	1.81	0.86	5.20	6.99	0.49	0.09
Minimum	1.10	0.88	0.44	0.21	2.67	1.23	22.91	15.59	0.09	0.05
Maximum	7.11	3.26	3.78	1.45	9.14	4.31	47.19	48.27	1.51	0.40

3.2.1. Dissolved Organic Carbon

During the RS, the DOC concentration averaged 3.42 ± 1.77 mg L^{-1} (n = 71), with the minimum recorded in the Ixcán River (M1; 1, 1 ± 0.01 mg L^{-1}) and the maximum in the San Pedro River (B1; 7.11 ± 0.32 mg L^{-1}). There was an increasing trend of DOC downstream (r^2 = 0.47; $p < 0.005$; Table 1; Figure 3a), with the highest values in the La Pasión (M7), San Pedro (B1), and San Pedro-San Pablo (B8) rivers. There were significant positive correlations between DOC and temperature (r = 0.95, $p < 0.001$), Chl-a concentration (r = 0.83, $p < 0.001$) and ORP (r = 0.64, $p < 0.001$), as well as inverse correlations with DO (r = −0.89, $p < 0.001$), pH (r = −0.85, $p < 0.001$), and turbidity (r = −0.57, $p = 0.01$). During the DS, the DOC average concentration was significantly (H = 9.6, $p = 0.002$) lower (1.7 ± 0.59 mg L^{-1}; n = 83) compared to the RS. The minimum and maximum values were found in the Ixcán (M1; 0.88 ± 0.02 mg L^{-1}) and the San Pedro rivers (B1; 3.26 ± 0.4 mg L^{-1}). DOC correlates positively with Chl-a concentration (r = 0.52, $p = 0.02$), TSS (r = 0.69, $p < 0.01$) and the K_{25} (r = 0.52, $p = 0.02$), and inversely with the DO (r = −0.63, $p < 0.01$). The DOC increased downstream, but the longitudinal trend was weaker compared with the RS (r^2 = 0.33, $p < 0.05$; Figure 3a).

The DOC concentration of the mainstem (M6, M8, M9, M10, B2, B3, B5, and B7) of both seasons was positively correlated with the discharge (r = 0.53, $p < 0.005$), and it is adjusted to a linear regression (y = 1.46 + 0.0004x; r^2 = 0.67, $p < 0.001$; Figure 3b).

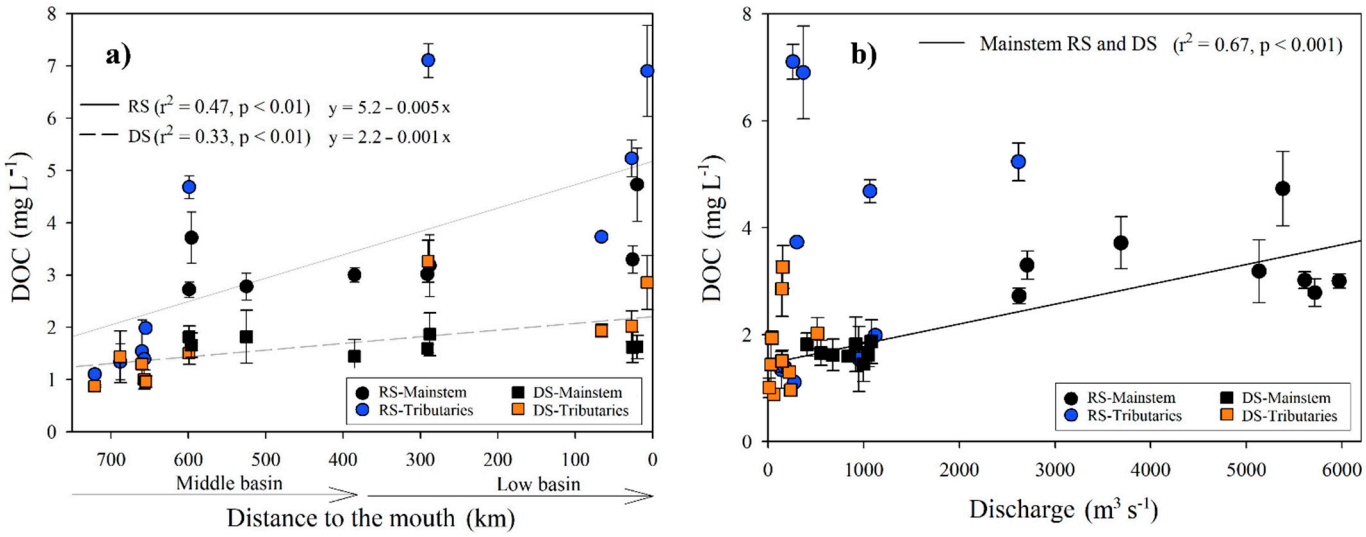

Figure 3. (**a**) Longitudinal variations in the DOC concentration (±SD) according to distance from the Usumacinta River's mouth during the rainy (RS) and dry (DS) seasons; (**b**) DOC adjustment regarding discharge into the mainstem of the Usumacinta River in the rainy (RS) and dry (DS) seasons. The mainstem differs in both seasons from the tributaries.

3.2.2. Particulate Organic Carbon

During the RS, the POC registered an average of 1.59 ± 0.85 mg L^{-1} (n = 72), with the minimum in the La Pasión River (M7; 0.44 ± 0.05 mg L^{-1}) and the maximum in the Lacantún River (M3; 3.78 ± 0.73 mg L^{-1}). There was only a positive correlation of POC with turbidity (r = 0.63, p < 0.01) and TSS (r = 0.7, p < 0.001). The POC in the RS was adjusted to a quadratic function (r^2 = 0.42, p < 0.05; Figure 4a) concerning the distance to the mouth. The maximum values were in the Lacantún River and tributaries (M1, M2, M3, and M5), which have high turbidity and TSS. Downstream, POC increases in the stations near the river mouth (B5, B6, B7, and B8; Table 1; Figure 4a).

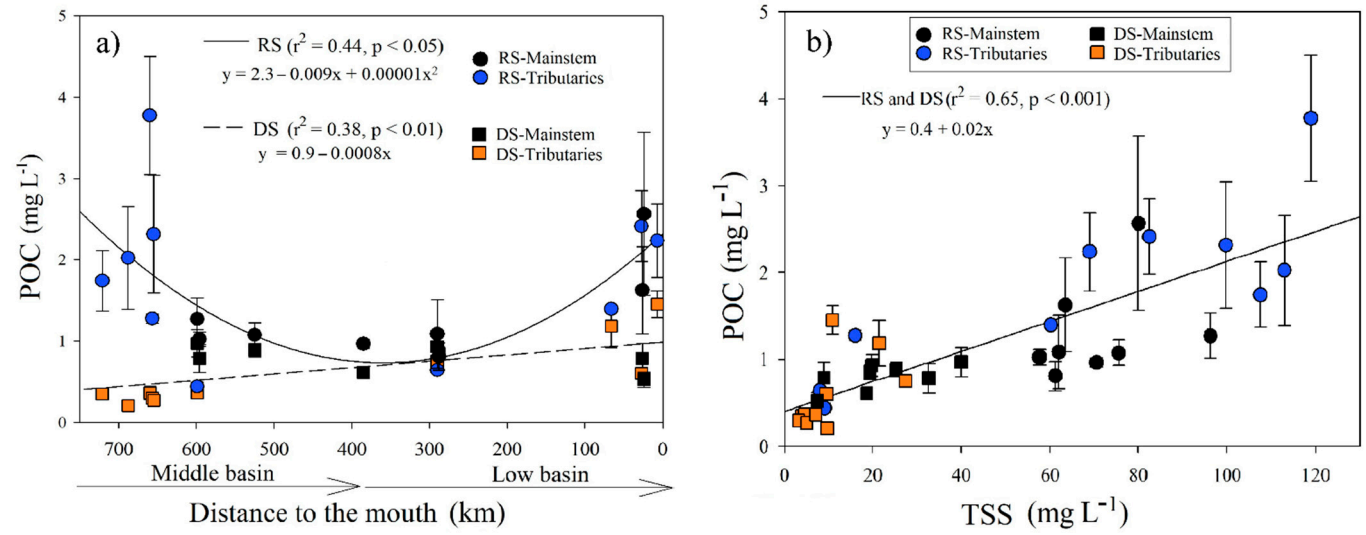

Figure 4. (**a**) Longitudinal variations in the POC concentration (±SD) according to distance to the Usumacinta River's mouth during the rainy (RS) and dry (DS) seasons; (**b**) POC (±SD) adjustment regarding total suspended solids concentration in the Usumacinta River in the rainy (RS) and dry (DS) seasons. The mainstem differs in both seasons from the tributaries.

The POC concentration was significantly lower (H = 15.1, $p < 0.001$) in the DS (0.68 ± 0.34 mg L^{-1}; n = 85) compared with the RS. The minimum and maximum values were found in the Chajul River (M2; 0.21 ± 0.01 mg L^{-1}) and the San Pedro-San Pablo River (B8; 1.45 ± 0.16 mg L^{-1}), respectively. The POC in the DS increased downstream (r^2 = 0.38, $p < 0.01$; Figure 4a) and presented positive correlations with the Chl-a concentration (r = 0.78, $p < 0.001$), TSS (r = 0.73, $p < 0.001$), DOC (r = 0.74, $p < 0.001$), and ORP (r = 0.6, $p < 0.01$).

In both seasons, POC showed a high dependence on the TSS concentration (r^2 = 0.65, $p < 0.001$; Figure 4b). The %POC (content in the TSS) in the Usumacinta River varied between 1.3% and 13.4% and was significantly (H = 11.5, $p < 0.001$) lower during the RS (2.9 ± 2.0%) compared with the DS (5.7 ± 3%). The variation that explains 60% of the variance of the % POC and TSS was fitted to a logarithmic function (Table S4; Figure S3).

The POC/Chl-a (mg C mg Chl-a^{-1}) ratio fluctuated between 107 and 10,362 (~1464 ± 2605), with significantly higher values (H = 8.7, p = 0.003) during the RS (Table S4). The POC/Chl-a ratio showed a decreasing trend until the river's mouth in a linear manner, both in the RS (r^2 = 0.34, $p < 0.05$), and in the DS (r^2 = 0.51, $p < 0.001$; Figure S4).

3.2.3. Total Organic Carbon

The TOC concentration during the RS ranged from 2.67 ± 0.07 mg L^{-1} in the Tzendales River (M4) to 9.14 ± 0.50 mg L^{-1} in the San Pedro-San Pablo River (B8), with an average of 5.01 ± 1.84 mg L^{-1}. A positive correlation was found with temperature (r = 0.75, $p < 0.001$), Chl-a (r = 0.71, $p < 0.001$), DO (r = −0.66, $p < 0.01$), and pH (r = −0.6, $p < 0.01$). During the DS, the TOC concentration was significantly (H = 19.9, $p < 0.001$) lower (2.38 ± 0.86 mg L^{-1}) than the RS. The minimum and maximum values were found at the confluence of the Lacantún with the Tzendales River (M5; 1.23 ± 0.06 mg L^{-1}) and the San Pedro-San Pablo River (B8; 4.31 ± 0.19 mg L^{-1}), respectively. In the DS, TOC was significantly correlated with TSS (r = 0.77, $p < 0.001$), Chl-a (r = 0.75, $p < 0.001$), and DO (r = −0.53, $p < 0.05$).

As shown in Figure 5a, TOC concentration increased downstream in both seasons, although the mainstem stations had a relatively constant concentration of TOC downstream. DOC was the most abundant TOC fraction in the Usumacinta River (Table S4). DOC represents ~66 ± 17% (29 to 92%) of TOC in the RS and ~72 ± 7% (62 to 87%) in the DS. During the RS, the POC in the Lacantún River (M3 and M5) and the Ixcán (M1), Chajul (M2), and Tzendales (M4) tributaries was the dominant fraction, while in the DS at the same stations, this proportion changed, dominated by the dissolved fraction (Figure 5b). In the middle (M6-M10) and lower basin (B1-B8), the DOC/POC ratio was >1, both for the RS (1.84–11.07) and for the DS (1.64–4.33), which shows that DOC is the main organic C fraction (Table S4). Additionally, the DOC/POC ratio was not statistically different between seasons (H = 0.4, p = 0.53). It did not present a longitudinal variation ($p > 0.05$) from the middle basin to the mouth in any sampling season.

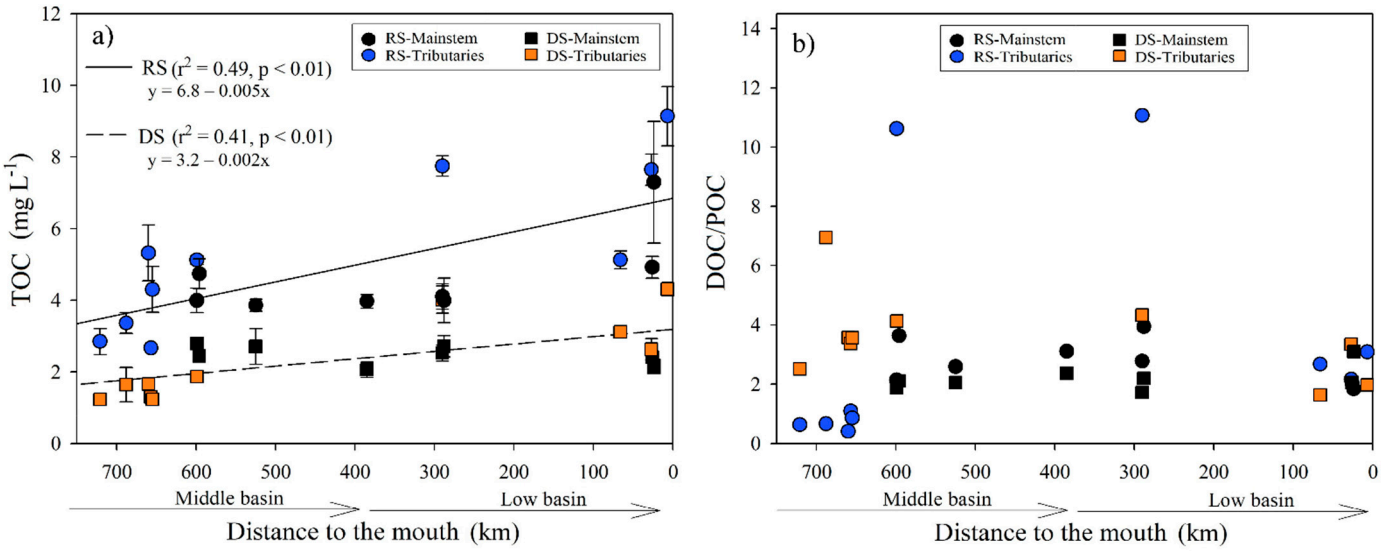

Figure 5. (**a**) Longitudinal variations in the TOC concentration (±SD) according to distance from the Usumacinta River's mouth during the rainy (RS) and dry (DS) seasons; (**b**) longitudinal variations in the DOC/POC ratio according to distance from the mouth of the Usumacinta River during the rainy (RS) and dry (DS) seasons. The mainstem differs in both seasons from the tributaries.

3.2.4. Dissolved Inorganic Carbon

During the RS, the average concentration of DIC was 30.1 ± 5.2 mg L^{-1} (n = 43), with the minimum value in the Chajul River (M2; 22.9 mg L^{-1}) and the maximum in the Tzendales River (M4; 47.2 mg L^{-1}). In the RS, there was only a positive correlation between DIC and K_{25} (r = 0.74, $p < 0.001$). For the DS, the DIC average concentration was slightly higher (33.1 ± 7.0 mg L^{-1}; n = 35), with the minimum in the Chajul River (M2; 15.6 mg L^{-1}) and the maximum in the La Pasión River (M7; 48.3 mg L^{-1}) (Table 1; Figure 6a). In the DS, there was a positive correlation between DIC and temperature (r = 0.66, p = 0.001). The DIC concentration in the two seasons was statistically different (H = 6.56, $p < 0.01$) and did not vary longitudinally ($p > 0.1$; Figure 6a). In addition, with a 95% confidence interval for the data mean (n = 36), DIC values fluctuated between 29.9 and 31.7 mg L^{-1}. The mean DIC/DOC ratio was significantly lower (H = 12.6, $p < 0.001$) during the RS (11.7 ± 7.7) compared with the DS (21.4 ± 7.7). In both seasons, there was a decrease in DIC/DOC ratios toward the river's mouth (Table S4; Figure S5).

3.2.5. Particulate Inorganic Carbon

The average concentration of PIC was higher in the RS (0.67 ± 0.49 mg L^{-1}) and lower in the DS (0.17 ± 0.09 mg L^{-1}), with statistically significant differences between sampling campaigns (H = 16.2, $p < 0.001$). During the RS, we measured the maximum (1.51 ± 0.38 mg L^{-1}) in the Chajul River (M2) and the minimum in the La Pasión River (M7; 0.09 ± 0.06 mg L^{-1}). PIC presented a decreasing trend downstream (r^2 = 0.29, $p < 0.05$) in the RS, but in the DS, PIC increased downstream (r^2 = 0.34, $p < 0.05$; Table 1; Figure 6b). The concentration of PIC was not related to the variation in the river flow in any season ($p > 0.05$), but it presents the same pattern of variation as the TSS (Figure S6). DIC was the dominant inorganic C in the Usumacinta River. It represents almost entirely dissolved inorganic C (97.7 ± 1.8% during the RS and 99.5 ± 0.3% in the DS).

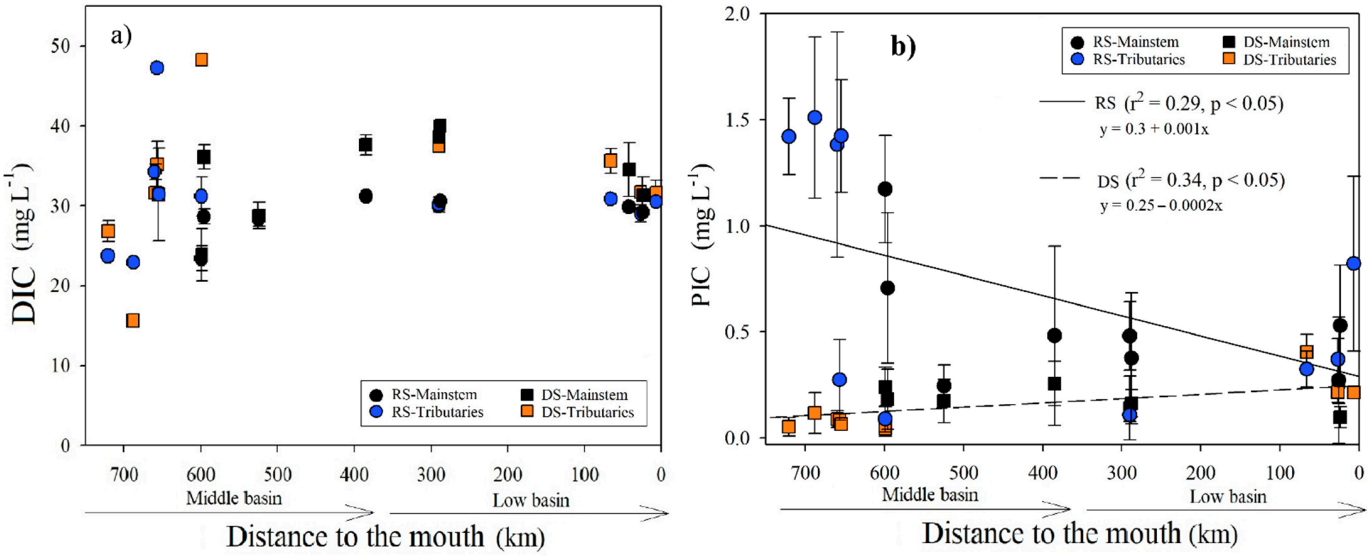

Figure 6. (**a**) Longitudinal variations in the DIC and (**b**) PIC concentrations (±SD) according to the distance to the Usumacinta River's mouth during the rainy (RS) and dry (DS) seasons. The mainstem differs in both seasons from the tributaries.

3.2.6. Total Carbon

DIC was the dominant fraction in both sampling seasons, followed by DOC, POC, and finally PIC (DIC > DOC >POC > PIC) (Figure 7).

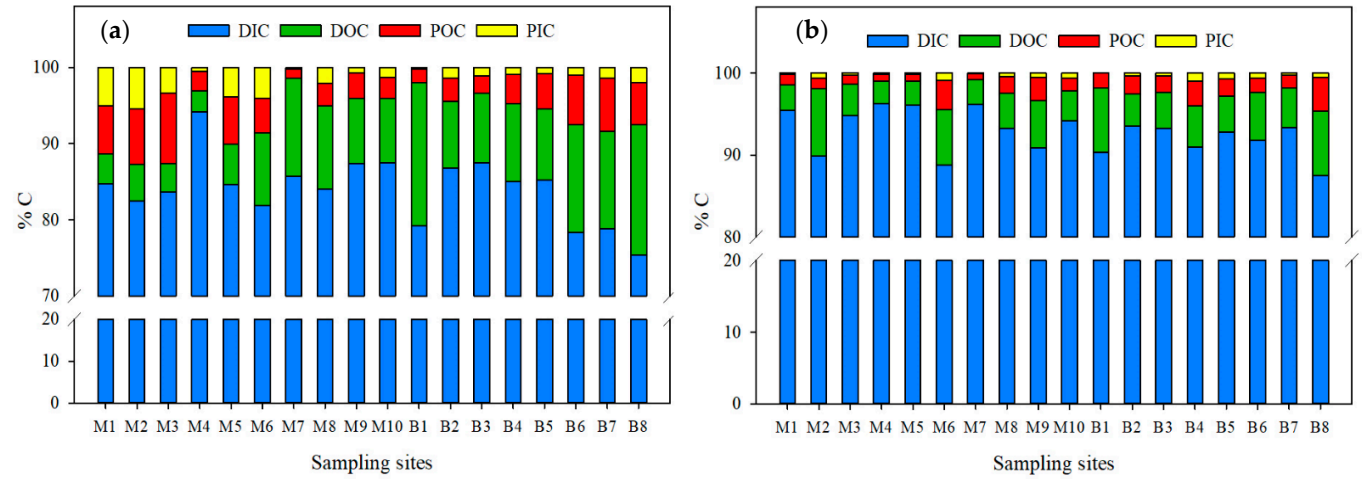

Figure 7. Percentage variations in C chemical fractions in the Usumacinta River during the (**a**) rainy and (**b**) dry seasons.

In the RS, the DIC averaged ~84 ± 4% (between 75% and 94%), followed by DOC (average of ~9.5 ± 4.5%, between 3% and 19%) and particulate fractions. However, in the Ixcán (M1) and the Chajul (M2) rivers, particulate C fractions were more abundant than DOC (DIC > POC > PIC > DOC). POC was the dominant organic fraction (DIC > POC > DOC > PIC) only in the Lacantún River (M3) and at the confluence with the Tzendales River (M5; Figure 7a). During the DS, the DIC averaged ~92.7 ± 2.6% (between 87% and 96%), followed by the DOC with ~4.9% ± 1.8% (between 3 and 7.9%). The particulate fractions measured a lower percentage (average of 1.9 ± 0.9% for the POC and ~0.5 ± 0.3% for the PIC; Figure 7b).

3.3. Instantaneous Carbon Fluxes

Calculated C fluxes were significantly higher in the RS: TOC ($H = 15.8$, $p < 0.001$), DOC ($H = 14.1$, $p < 0.001$), POC ($H = 13.2$, $p < 0.001$), and DIC ($H = 9.2$, $p = 0.002$). In addition, C fluxes showed a high correlation with Q (r = 0.9, $p < 0.001$), demonstrating that C export is highly conditioned by water discharge rather than by the concentration of each C fraction. Table S5 shows the averages (±SD) of the DOC, POC, TOC, and DIC fluxes calculated at the 18 sampling sites of the Usumacinta River.

During the RS, the mean TOC flux (1032 ± 956 t d^{-1}) was two orders of magnitude higher than in the DS (93 ± 84 t d^{-1}). Notably, in the La Pasión River sub-basin (M7), the TOC flux was ~20 times greater in the RS than in the DS. The DOC flux represents ~66 to 72% of the TOC flux (Table S4). However, in the Lacantún River (M1-M5), POC represents ~70%, although during the DS, the DOC flux is again dominant (~71% to 87%). The Chixoy (M6) and San Pedro (B1) rivers are the tributaries that contribute the highest and lowest OC loads, respectively (Table S5). Specifically in the DS, the Chixoy River (M6) has a TOC flux contribution ~four times higher than the other major tributaries. The highest OC fluxes during the RS occurred at the confluence of the Grijalva River (B7) with the Usumacinta River, despite having a lower Q than the Boca del Cerro station (M10; Table S2). In the DS, the maximum OC flux occurs at the confluence of the San Pedro River (B3; highest flow measured) with the Usumacinta River and decreases until the river's mouth.

DIC flux accounted for the most significant percentage of total C load in both the RS (~84 ± 4%) and the DS (~93 ± 3%). The Chixoy River sub-basin (M6) contributed the highest amount of DIC flux into the mainstem in both the RS and DS. However, DIC transport was ~6 times higher in the rainy season (Table S5) even though the concentration measured between both seasons was practically similar (23.4 mg L^{-1} versus 23.8 mg L^{-1}). This behavior corroborates the importance of hydrology in transport. The Tzendales River (M4) has peculiar comportment because DIC flux was ~15 times higher in the RS (Table S5) compared with the remaining stations (~5 times more). In addition, M4 transported the highest percentage of DIC (94% at RS and 96% at DS) relative to the OC fractions.

3.4. C Balance in the Lower Basin of the Usumacinta River

The C inflow–outflow mass balance in the RS was positive for all C species, showing net retention (C sink) within the river reach. DOC, POC, TOC and DIC fluxes decreased downstream with respect to Boca del Cerro (M10), approximately ~36%, ~9%, ~30%, and ~50%, respectively (Table 2).

Table 2. Balance of water discharge (Q) and C fluxes in the Usumacinta River basin and the total C export to the Gulf of Mexico in the rainy (RS) and dry (DS) seasons. (See Figure 1 and Table S1 for the detailed locations of the sampling sites).

	Code	Q		DOC Flux		POC Flux		TOC Flux		DIC Flux	
		(m^3 s^{-1})		(t d^{-1})		(t d^{-1})		(t d^{-1})		(t d^{-1})	
		RS	DS	RS	DS	RS	DS	RS	DS	RS	DS
Input	M10	5970	998	1549.0	124.8	497.7	52.8	2046.8	177.7	16,073.4	3240.4
Output	B5	2709	677	771.8	94.6	380.0	46.0	1151.8	140.6	6988.9	2018.0
	B8	368	146	219.7	36.0	71.2	18.3	290.9	54.3	970.4	398.5
Balance (input−output)	M10 − (B5 + B8)	2893	175	557.5	−5.8	46.5	−11.5	604.1	−17.2	8114.1	823.9
Usumacinta basin export	B5 + B8	3077	823	991.5	130.6	451.2	64.3	1442.7	194.9	7959.3	2416.5
Usumacinta-Grijalva	B7	5380	1048	2198.8	146.9	1192.9	47.5	3391.8	194.4	13,557.9	2830.2
Usumacinta-Grijalva basin export	B7 + B8	5748	1194	2418.5	182.9	1264.1	65.8	3682.7	248.7	14,528.3	3228.7

In contrast, in the DS, the balance was negative. DOC, POC, and TOC fluxes increased (~5%, ~22%, and ~10%, respectively) from the middle basin (M10) to the lower basin (B5 plus B8). Differently, the DIC flux in the DS decreased ~25% concerning the gauging station

M10 (Table 2). The lower Usumacinta River basin is a sink for DIC in both seasons, with this function being greater in the RS.

The Grijalva River (B6) contributes significant amounts of C to the Usumacinta River that further discharges to the southern Gulf of Mexico. During the RS, the daily fluxes of DOC, POC, TOC, and DIC from the Grijalva River (B6) represents ~59%, ~64%, ~61%, and ~45%, respectively, of the discharge of the entire basin (B7 + B8; Table 2; Figure 8a). On the contrary, in the DS, the percentage of the Grijalva River (B6) contribution decreases substantially, with ~29%, ~2%, ~22%, and ~5% of the DOC, POC, TOC, and DIC fluxes, respectively (Table 2; Figure 8b).

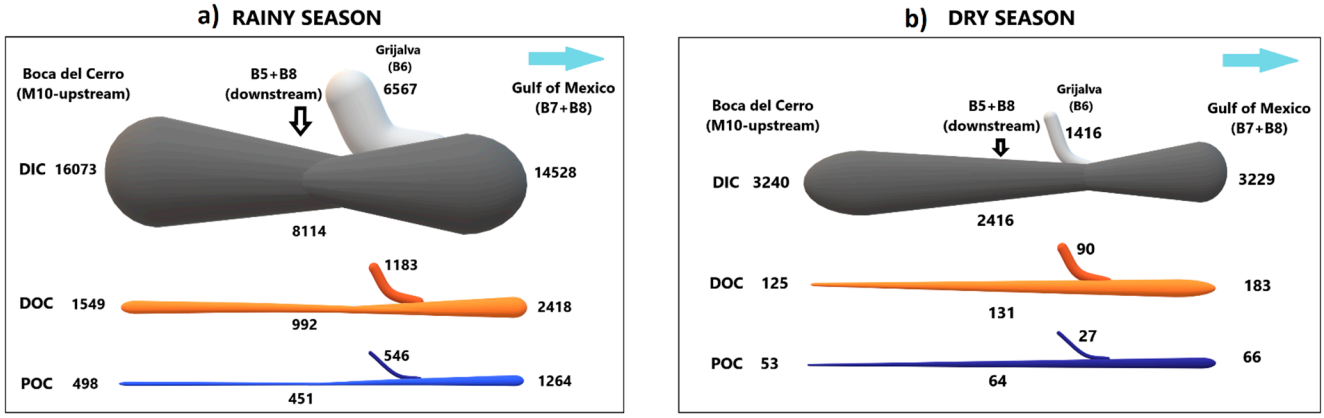

Figure 8. Application of the conceptual framework to the carbon flux (t d^{-1}) balance during the (**a**) rainy and (**b**) dry seasons in the lower basin of the Usumacinta River. The widths of the lines, proportional to the magnitude of the fluxes, are consistent within one season but not between the different seasons.

In the RS, the DOC export to the southern Gulf of Mexico was ~13 times higher (2418.5 t C d^{-1}), ranging from 1914 to 2954 t C d^{-1}. Meanwhile, in the DS, the DOC flux averaged 182.9 t C d^{-1} (from 155 to 229 t C d^{-1}). On the other hand, the daily POC efflux can increase up to ~19 times higher at RS (1264.1 t C d^{-1}; from 904 to 1970 t C d^{-1}) compared with the DS (65.8 t C d^{-1}; from 50 to 81 t C d^{-1}). Finally, the DIC efflux to the Gulf of Mexico in the RS was 14,528.3 t C d^{-1} (from 14,447 to 14,593 t C d^{-1}), which was almost 4.5 times higher than the DS (3228.7 t C d^{-1} (from 3074 to 3391 t C d^{-1}) (Table 2).

According to the C flux balance (Table 2; Figure 8) between the gauging station (M10) and the outlet (B7 + B8), the fluxes of DOC (1.5 to 1.6 times), POC (1.2 to 2.5 times), and TOC (1.4 to 1.8 times) increase at the river mouth. Meanwhile, the final DIC flux decreases slightly (0.9 times) concerning Boca del Cerro (M10). The previous balance (M10 vs. B7 + B8) indicates that the dynamics of the lower basin (with wetland and floodplain systems) and the contribution of the Grijalva River (B6) are fundamental to quantifying the final C load to the Gulf of Mexico. However, it must be considered that in the dry season, the seawater intrusion could modify the C export to the sea of the Usumacinta River; nonetheless, the seawater intrusion reaches only the stations closest to the river's mouth. On rainy season, there is no seawater intrusion.

3.5. Annual C Loads Estimates

The Usumacinta River at Boca del Cerro (M10) transports an estimated total of 0.194 ± 0.015 Tg DOC (0.180 to 0.215), 0.066 ± 0.004 Tg POC (0.062 to 0.070), 2.571 ± 0.076 Tg DIC (2.541 to 2.606), and 0.032 ± 0.024 Tg PIC (0.016 to 0.064) for the study period (2017–2018).

Considering the balance between Boca del Cerro (M10) and the rivers' mouths (B7 and B8; Table 2; Figure 8), the Usumacinta-Grijalva system (HR-30) discharges to the Gulf of Mexico ~0.294 ± 0.013 Tg DOC yr^{-1} (0.265 to 0.336), ~0.125 ± 0.06 Tg POC yr^{-1} (0.077 to 0.180), ~2.443 ± 0.167 Tg DIC yr^{-1} (2.297 to 2.596), and 0.026 ± 0.012 Tg PIC yr^{-1} (0.008 to 0.034). Overall, the annual C export of HR-30 during the study period was estimated

at ~2.879 Tg C yr^{-1} (2.648 to 3.146), of which DIC accounts for 85% of the total flux, followed by DOC (10%), POC (4%) and a minimal fraction (<1%) corresponding to PIC. The calculated yields of DOC, POC, and DIC for the Usumacinta-Grijalva system were 2.61 t km^2 yr^{-1} (2.36 to 2.99), 1.11 t km^2 yr^{-1} (0.69 to 1.59), and 21.70 t km^2 yr^{-1} (20.41 to 23.07), respectively. The latter is the first estimate of C transport (organic and inorganic) to the ocean for a Mexican tropical lotic system. The results can be incorporated as a baseline for further, more elaborate, more accurate studies and for modeling the regional C budget.

4. Discussion

4.1. Temporal and Spatial Variation of C in the Usumacinta River

4.1.1. Comparison with Other Large Rivers

The average concentrations of DOC measured in the Usumacinta River in the RS (3.4 ± 1.8 mg L^{-1}) and the DS (1.7 ± 0.6 mg L^{-1}) were lower than the estimate of the world DOC average (~5.75 mg L^{-1}) [88]. The rivers of the tropical zone usually have DOC values between 2 and 15 mg L^{-1}, with average values of 7.4 mg L^{-1} in Africa, 4.9 mg L^{-1} in America, 5.2 mg L^{-1} in Asia, and 4.8 mg L^{-1} in Oceania [11]. In rivers that drain carbonate rocks, such as the Usumacinta River, the concentration of DOC is more limited (~1 mg L^{-1}) [12]. Other tropical rivers report similar DOC values to this study (Table 3), for example the Zambezi, southern Africa (1.2 to 4.9 mg L^{-1}) [89]; the Tana, Kenya (0.2 to 6.9 mg L^{-1}) [47]; and the Orinoco, Venezuela (1.7 at 4.1 mg L^{-1}) [38]. Higher DOC values in rivers are associated with larger wetlands and conserved forests [25]. Certain tropical rivers have DOC values greater than 10 mg L^{-1}, for example the Negro River, Brazil (12.7 mg L^{-1}) [25], and the Nyong River, Cameroon (6.4–51.0 mg L^{-1}). These colored waters have large amounts of humic substances and high dissolved OM content [90].

Table 3. C concentrations in tropical rivers around the world. The temperate Mississippi River, which also discharges into the Gulf of Mexico, was included for comparative purposes. (* Data from [91]. The average and range are shown).

River	Watershed Area × 10^6 (km^2)	Q * (m^3 s^{-1})	C (mg L^{-1})			Reference
			DOC	POC	DIC	
Usumacinta	0.07	15 to 5970	2.56 (0.88–7.11)	1.14 (0.21–3.78)	31.6 (15.6–47.2)	This study
Amazon	6.30	209,000	5.65 (3.4–10.25)	1.25 (0.44–4.46)	1.4	[25,92]
Congo/Zaire	3.80	42,000	7.78 (3.5–11.8)	1.57 (0.7–2.3)	3.1	[25,93]
Mississippi	3.30	18,074	3.7 (2.9–4.1)	4.3 (1.9–9.7)	29.1 (19.2–41.4)	[18,31]
Orinoco	1.10	34,880	2.92 (1.75–4.12)	0.91 (0.24–2.29)	2.0	[38,77]
Irrawaddy	0.43	12,049	1.2–2.9	1.2–5.2	23.6	[45,77]
Negro	0.68	28,400	12.7 (3–18)	0.72 (0.26–1.09)		[92]
Zambezi	1.30	3171	1.2–4.9		6.3	[77,89]
Godavari	0.31	2917	1.3–4	7.2 (0.3–20)	34.8 (6–53)	[94,95]
Red	0.15	2109	2.0 (0.1–8.5)	1.5 (0.1–9.0)	19.6 (9.1–29.9)	[54,55]
Senegal	0.27	697	2.1 (1.25–3.25)	0.2–4.0		[50,77]
Nyong	0.03	193	16.0 (6.4–51)		3.77 (1.6–8.1)	[96]
Maroni	0.07	1807	5.8 (2.12–11.34)	1.8 (0.45–4.5)		[97]
Tana	0.04	150	0.2–6.9	0.3–120	13.2 (2.4–57.6)	[47,48]

The average POC of the Usumacinta River ~1.1 mg L^{-1} (0.2 to 3.8 mg L^{-1}) is lower than that reported for North American rivers with ~2.5 mg L^{-1} (1 to 10 mg L^{-1}) but like other tropical rivers (Table 3) such as the Maroni, French Guiana [97], and the Apure and Orinoco, Venezuela [38]. Some highly turbid tropical rivers with high TSS loads (>100 mg L^{-1}) have higher POC concentrations than the Usumacinta River. This is the case for the Tana, Kenya (0.8 to 141.9 mg L^{-1}) [49]; and the Yellow, China (4.6 to 92.4 mg L^{-1}) [98] (Table 3).

DIC in the Usumacinta River averaged 31.6 ± 6.3 mg L^{-1} (15.6 to 48.3 mg L^{-1}; Table 1). According to Cai [99], the maximum DIC (as HCO_3^-) of large rivers globally is ~3115 µmol L^{-1} (37.4 mg L^{-1}), for the Danube River, Central Europe. Other large rivers on carbonate lithology such as the Yellow (~2591 µmol L^{-1}, 31.1 mg L^{-1}), the Mississippi,

USA (~2421 ± 480 µmol L^{-1}, 29.0 ± 5.8 mg L^{-1}), and the Godavari, India (~2156 µmol L^{-1} or 25.9 mg L^{-1}), have DIC values greater than 25 mg L^{-1} [18,99] (Table 3).

The DIC values for the tropical zone are low due to the lower percentage of carbonate rocks [11]. The average riverine DIC for tropical America is 434 µmol L^{-1} (5.2 mg L^{-1}). In Africa (395 µmol L^{-1} or 4.74 mg L^{-1}) and equatorial Asia (1064 µmol L^{-1} or 12.8 mg L^{-1}), DIC values are also low but increase toward high latitudes (>30° N) [11]. Our DIC results place the Usumacinta River among the highest concentrations reported in the world's large rivers [12]. Considering that the Mississippi River is not included as a tropical river [11], the present study reports that the highest DIC loads in rivers of tropical America are represented by the middle and lower basin of the Usumacinta River. This value is higher than other large tropical rivers (Table 3), such as the Amazon, Brazil (4.1 mg L^{-1}) and the Orinoco (2.0 mg L^{-1}) and Paraná, in the south of south America (3.4 mg L^{-1}), which have less than 4% carbonate rocks [100,101].

Our DIC results are higher than those reported in the global river discharge database (GEMS-GLORI) for the Usumacinta (value at Boca del Cerro–M10; 27.7 mg L^{-1}) and the Grijalva (25.4 mg L^{-1}) [77]. Although there are scarce and scattered DIC reports from other Mexican rivers [e.g., Ameca (17.7 mg L^{-1}), Balsas (32.7 mg L^{-1}), Pánuco (35.0 mg L^{-1}), Grande/Bravo (31.4 mg L^{-1}) [77]], the present investigation is the first describing the spatiotemporal patterns of DIC concentrations in a Mexican river and its most important tributaries.

The Tzendales (M4; 41.2 mg L^{-1}) and La Pasión (M7; 39.7 mg L^{-1}) rivers presented the highest DIC averages in the two sampling seasons. The preceding can be directly associated with the lithological characteristics of each sub-basin: the La Pasión River (M7) has ~66% Cretaceous carbonates, and agricultural activities in the Guatemalan part possibly increase the DIC due to liming. Meanwhile, the Tzendales (M4) drains from a steeply sloping limestone zone. High and similar ranges of DIC have been reported in rivers from small karst basins such as the Houzhai River, China (30.2 to 70.2 mg L^{-1}) [57], and the Mascouche River (19.0 to 61.4 mg L^{-1}; a tributary of the St. Lawrence River, Canada) [102].

4.1.2. Correlation between DOC, POC, and DIC and Water Discharge

According to Degens [103], DOC increases during the rainy season due to (i) the processes of leaching and dragging of OM through surface soil erosion ("flushing effect"), (ii) the infiltration of OM and the microbial degradation of the flooded terrestrial vegetation, and (iii) by the C processing from the floodplain. DOC in the RS should be primarily allochthonous. Thus, in the DS, the input of allochthonous OC must decrease enormously, and the DOC loads would be dominated by the in situ contribution and POC transformations [12]. This hypothesis, which seems feasible, must be verified using stable isotopes. The increase in DOC as rainfall increases (Figure 3b) has been seen in several rivers worldwide, such as the Nyong [96], Zambezi [89], Senegal, West Africa [50], Mississippi, [18], Maroni [97], Orinoco, [38], Amazon, and Congo, the Democratic Republic of Congo [25,43].

The POC in the Usumacinta River showed a positive relationship with the TSS (Figure 4b), like that previously reported by Cuevas-Lara [42] in 2017. According to Seyler [25], the variation of TSS and POC depends on the hydrology and land use of the drainage basin. Mechanical erosion increases during precipitation events and mobilizes particulate material from riparian zones or associated with soil clay minerals. The increased discharge also removes sediment and C from the bottom of the channel, thus increasing turbidity [12]. According to Muñoz-Salinas [71], cyclonic storms during the rainy season in the Usumacinta-Grijalva system promote the entrainment of large volumes of OM and sediments due to episodes of high erosion around the watershed.

The positive relationship between POC and TSS (Figure 4b) has been reported in most lotic systems worldwide [12,26], both in tropical rivers of South America [38,92,97,100], Asia [55,98], Africa [25,43,49] and in rivers of temperate zones [104]. Few studies report a PIC–TSS relationship such as in the Usumacinta River (Figure S6). However, PIC shows a similar trend to POC in rivers worldwide [34,103].

Several river systems [38,52,92,97] reported a decrease in %POC with increasing TSS loads, as was observed in the Usumacinta River (Figure S3). This variation may depend on various processes such as POC dilution by increasing mineral material in highly turbid rivers. At the beginning of the rainy season, erosive processes occur in the surface horizons of the soil with high OC content. Meanwhile, sediments are removed from the deepest soil horizons (refractory OC) if erosion rates increase, generating a lower % POC in TSS [52]. Thus, if the concentration of TSS is low (dry season), the POC must come from the superficial horizons of the soil and aquatic PP [42]. On the other hand, when the TSS loads are higher (rainy season), the POC must come from deep soils and sedimentary rock, generating a lower % POC [105].

Previous studies [29,35,103] have demonstrated an inverse relationship between DIC concentrations and discharge rates in many rivers. This pattern is explained by a dilution effect, variations in C sources, and the balance between rainfall and evaporation [106]. In most of the sampling stations on the Usumacinta River, the DIC was higher during the DS, except in the Lacantún River sub-basin (M2, M3, M4, and M5; Table 1). Thus, DIC's concentration effect is generated during the DS due to low rainfall and higher temperature and evaporation. A similar pattern has been reported in tropical [65,99,107,108] and subtropical [109] rivers. According to Cai [99], the concentration of HCO_3^- in the principal worldwide rivers is negatively correlated with the discharge. This pattern suggests that the DIC concentration is more related to the balance of precipitation–evaporation in the drainage basin. In addition, the Mississippi River, which has a low content of carbonate rocks (18%), has a high concentration of dissolved HCO_3^- in the water and moderate DIC fluxes. Consequently, it is inferred that the high concentration of DIC results at least partially from the loss of water by evaporation [99]. Similarly, in the Changjiang River, China, the highest concentrations of ions (Ca^{+2}, Mg^{+2}, and HCO_3^-) occur during the lowest discharges. The latter is important to mention because the increase in discharge into the Usumacinta River, up to six times more during the rainy season, would be expected to dilute the concentrations of these main ions significantly, and in fact, Olea-Olea et al. [85] reported significantly higher ion values during the dry season. In addition, they mention that geochemical models show that the main weathering of carbonate rocks in the dry season and carbonate and silicate rocks in the rainy season handle the chemistry of the Usumacinta River.

The studies that prove a corresponding seasonal increase in DIC loads with river discharge are limited [110]. In the Chajul (M2), Lacantún (M3 and M5), and Tzendales (M4) rivers, the DIC was higher in the RS. Hence, the concentration of DIC may depend on the frequency and intensity of precipitation in specific karst basins. Qin [57] recorded higher DIC values in the rainy season of the Houzhai River Basin, China. These results highlight that rainfall promoted the exchange between surface water and groundwater (increased contribution of CO_2 from the soil) through the highly transmissive karst aquifers with underground drainages [111].

4.1.3. Spatial Variation of DOC, POC, and DIC Concentrations

In the Usumacinta River basin, the general trend in DOC is to increase from the middle basin toward the river's mouth, in the RS (Figure 3a), as reported in the Amazon River basin by Hedges [112], who mentions that DOC has an inverse relationship with altitude. In the Cuibá River basin, Brazil, [113] reported a longitudinal increase in DOC concentration from the upper region (plateau river) to the El Pantanal wetland zone. Due to the hydrological connectivity, this trend was more pronounced in the rainy than in the dry season. Another similar case is the Zambezi River [89], which presented a longitudinal increase in DOC concentration from the upper part to the mouth at the Indian Ocean during the rainy season, associated with a high correlation with the wetland extension. During the dry season, when there is low hydrological connectivity, the DOC gradually decreases toward the river's mouth [89]. In other rivers, such as the Mississippi, the DOC gradually decreases downstream because of constant dilutions of the tributaries that have

lost wetlands due to changes in land use [67]. According to Meybeck [12], shallow wetlands and peat bogs are the primary sources of riverine DOC. Although there is a DOC increasing trend downstream, the DOC concentration in the mainstem remains relatively constant until the confluence with the Grijalva River, which increases the concentration of DOC, mainly in the RS.

The flooding zone in the lower basin of the Usumacinta River and the wetland complex (La Libertad, Catazajá, and Pantanos de Centla-CWBR) [114] have significant effects on the increase in DOC in the RS. The highest DOC values (Table 1; Figure 3) in the San Pedro River (B1) are associated with Laguna del Tigre National Park (Guatemala, RAMSAR site N° 488). It is an extensive alluvial plain of wetlands (temporal ponds and permanent lakes) and the rainiest part of the Yucatán Peninsula [115]. Similarly, in the La Pasión River sub-basin (M7), the DOC is likely to increase because El Pucté Wildlife Refuge (167 km^2) is near the sampling station. It is part of the protected areas of southern Petén, characterized by floodplains, forests, lowlands, wet marshy areas, and water springs [116].

The stations of the Lacantún River (M1, M2, M3, M4, M5) have the lowest DOC values (<2 mg L^{-1}; Table 1; Figures 3a and 7). These sub-basins have a limestone lithology (~50%) and rainforest cover (~65%) associated with the Lacandona forest and the RBMA. Leptosol is the most abundant soil group. These soils are shallow, rocky, and poorly developed, with a large amount of calcareous material and low amounts of OM [117,118]. These characteristics of the sub-basin explain the lowest DOC concentrations recorded, considering that pristine rivers [119] from carbonate basins [12] and with low soil OC content [16] usually have low DOC concentrations (1 to 3 mg L^{-1}).

Meybeck [12] uses the relationship between %POC and TSS to differentiate fluvial POC. The autochthonous POC may be more meaningful if the TSS concentration is <10 mg L^{-1}. In addition, the POC/Chla-a ratio can be a good indicator of fluvial OC sources. For example, if the ratio POC/Chl-a is ~50 (30–100; average value for phytoplankton), the POC is autochthonous, but if the ratio is >200, the POC originates from erosion and runoff from the basin [105,120]. The average POC/Chl-a ratio in the Usumacinta River was 1465 ± 2605 (from 108 to 10,362), with higher values in the RS (~6 times higher) and a decreasing trend toward the river's mouth (Figure S4). Our results indicate that the POC is typically soil-derived. Some tropical rivers present more extreme POC/Chl-a ranges, such as the Tana (75 to 40,781) [47] and Red, Vietnam (23 to 9413) [55], reflecting, in the same way, the terrestrial sedimentary origin.

The La Pasión (M7) and San Pedro rivers (B1) showed low TSS values (<10 mg L^{-1}; Tables S2 and S3) and a POC/Chl-a ratio (342 and 158, respectively) at the other sampling stations (Table S4; Figure S4). M7 and B1 have a comparatively higher autochthonous contribution in the rainy season. On the other hand, at the Lacantún River stations (M1, M2, M3, M4, and M5), the POC/Chl-a ratio presented the highest values. These results show that the more significant drag of terrestrial material during precipitation events generates an increase in turbidity and a reduction in aquatic PP [121]. In contrast, the POC/Chl-a ratio at the stations near the river's mouth (B5, B6, B7, and B8) shows that the autochthonous contribution (phytoplankton) is essential, comprising up to 50% of the POC during the dry season, due to the marine contribution and the lower turbidity that favors the PP [42]. Something similar occurs in the Senegal River's marine-influenced area, where high concentrations of phytoplankton were found [50]. However, it is necessary to identify the POC sources using stable isotopes of C ($\delta^{13}C$), as reported in other river systems.

According to Wetzel [122], the riverine DOC/POC ratio depends on the relief of the basin, and it is usually between 6:1 and 10:1. This ratio shows that most of the transported riverine OC is dissolved. Globally, the mean DOC/POC ratio is ~1.2 [26], with minimum values (<1) for mountain or highly turbid streams [98] and maximum (>20) for highly polluted rivers or with minimal contributions of particulate matter [88].

At the Lacantún River stations (M1, M2, M3, M4, and M5) during the RS, the DOC/POC ratio is <1 (Table S4; Figure 5b). In particular, the Tzendales River (M4) has the lowest amount of DOC (~29%). In humid tropical regions with mountainous relief, such as the

upper basin of the Amazon River [12], or some Asian monsoon rivers [123], the DOC/POC ratio is <1. The steep slopes (30–65%) and precipitation (~3000 mm yr^{-1}) [124] of the Lacantún River are the principal erosivity factors. That influences our study's highest concentration of sediments (Table S2) and POC (Figure 4a).

In the remaining stations in the middle (M6–M10) and lower (B1–B8) basins, the DOC/POC ratio in both seasons was >1 (Table S4; Figure 5b). This ratio is like in other tropical rivers, such as the Congo and the Amazon, which have a significant contribution (~80%) of DOC derived from the decomposition of OM in wetlands and natural forests [25]. Notably, the La Pasión River (M7) and the San Pedro River (B1) presented the highest DOC/POC ratios in the entire basin (Table S4; Figure 5b). These ranges suggest similar behavior to the Negro River [25], which has high DOC (93%) with humic substances from highlands and flooded forests [125] as well as acidic pH (3.0 to 5.5). However, the La Pasión (M7) and San Pedro rivers (B1) presented a pH of ~7.4, so it could be inferred that there is no high concentration of humic substances. Still, due to wetlands and grassland areas, the DOC was higher (~86%) than in the mainstem and other tributaries of the Usumacinta River.

The DIC concentration did not present a pattern of longitudinal variation in the Usumacinta River. However, the seasonal variation was more marked in the middle basin than in the stations near the rivers' mouth (Figure 6a), possibly due to the higher precipitation and slope promoting greater weathering. In other rivers, such as the Rhône, France [126], or the Tana [48], there is an increase in DIC from the headwaters to the river's mouth. This longitudinal variation depends on lithology (a higher percentage of carbonate rocks in the lower catchment) and erosion in the drainage basin. DIC loads may also decrease downstream due to the dilution effects of tributaries with less carbonate rock cover (Yangtze River, China) [123].

The dynamics of a tropical river are highly dependent on precipitation and flow rates [36]. In our study, there was an increase in Chl-a (>PP) during the DS (Figure S2) associated with lower TSS input (Tables S2 and S3), turbidity, and flow velocity. For this reason, an increase in DIC consumption from photosynthetic activity in the dry season (low DIC/DOC) would be expected. However, in the Usumacinta River, the variables of river metabolism seem to have little importance in regulating DIC, with more influence on the rainfall–evaporation balance or CO_2 evasion. The DIC's biological (PP or R) contribution in karst catchments is considerably lower than in non-karst systems [57].

4.2. C Balance in the Usumacinta Lower Basin

According to the mass balance (Figure 8), the wetland and floodplain system of the lower basin (CWBR, Figure 1) is a C sink during the RS, retaining 557.5 t d^{-1} DOC and 46.5 t d^{-1} POC. Contrarily, the lower basin during the DS acts as a source of C, mobilizing 5.8 t d^{-1} DOC and 11.5 t d^{-1} POC (Table 3). The DIC flux balance is positive and indicates that the lower Usumacinta River basin acts as a net sink of DIC in both seasons (8114.1 t d^{-1} in the RS and 823.9 t d^{-1} in the DS).

Floods can overflow the Usumacinta River's mainstem, and a significant fraction of the OC can be retained in the adjacent floodplains. According to [127], flow connectivity with adjacent lakes and wetlands increases strongly in the lower basin of the Usumacinta River during the RS. Estrada et al. [128] mention that during floods, the area of wetlands in the lower basin around the Usumacinta and San Pedro rivers (B1) increases up to 2.48 times compared with the driest season. Few studies have addressed the ecological functioning of the Usumacinta River floodplain lakes [129,130]. Nevertheless, according to [130], differences in water quality (nutrients, sediments, and Chl-a) suggest that floodplains may be sediment sink areas and contribute OM to the river.

During the rainy season, the organic C can be deposited in the floodplains (POC) or mineralized (DOC), emitting considerable amounts of CO_2 into the atmosphere, as observed in other rivers [68,106]. The downstream decrease of ~50% of DIC fluxes (Figure 8) indicates a greater amount of CO_2 evasion in this zone, supporting the latter assumption. On the other hand, during the dry season, the lower basin of the Usumacinta River acts as a

DOC and POC source. In addition, since the Chl-a concentration increases downstream (Figure S2) and the POC/Chl-a ratio decreases (Figure S4), the autochthonous contribution of organic C in the dry season must be an essential contributor to the C fluxes, mainly POC, as previously mentioned [42]. However, it is important to mention that the DIC/DOC ratio (Figure S5) also decreases downstream in the dry season. The latter may be related to the PP processes that consume inorganic C.

Rivers can store sediment and OM in the channel, floodplains, and other depositional areas [131]. For example, [51] mention that the Tana River retains TSS and C (DOC, POC, and DIC) over 385 km between sampling stations. Moreover, as flow increases, POC retention also increases, and DOC retention decreases, although the fate of the retained C is unknown. Recently, wetlands in the Amazon River basin were found to accumulate significant amounts of C and are an essential component of the fluvial C budget of tropical rivers [132]. Future work in the Usumacinta River must analyze C's fate and the wetland zone's importance (CWBR) in the C budget.

4.3. Global C Export from the Usumacinta-Grijalva River to the Gulf of Mexico

The total estimated C loading into the southern Gulf of Mexico calculated for the Usumacinta-Grijalva was 2.879 Tg C yr^{-1}. This value represents the first estimate of C flux from the largest tropical river in Mesoamerica. Li [16] re-estimated the C flux in 263 river systems globally and determined that flow is the main factor modifying the fluxes of DOC, POC, and DIC. This model does not consider the impact of human activities (e.g., land-use changes, dams, water consumption, sewage input, and sediment dredging) in the drainage basin, so there may be uncertainties in the estimates of C fluxes. However, it is essential background for our study.

The DOC flux calculated for 2017–2018 in the Usumacinta-Grijalva system was higher than the [16] model (0.29 Tg C yr^{-1} versus 0.25 Tg C yr^{-1}). This behavior can be associated with the increase in DOC concentration in the lower basin due to the contribution of the wetlands systems such as the Pantanos de Centla, as previously described. In addition, the Grijalva River (B6) contributes considerably more DOC than the Usumacinta River during the RS (Table 2). This supply may be associated with a higher degree of deforestation and extensive agricultural and livestock activities in the middle and lower Grijalva River basins [133], as well as the presence of two large cities (Tuxtla Gutierrez and Villahermosa) that modify the water quality of the Grijalva River [74,134].

The POC flux in this study is ~three times lower than the [16] model (0.07 to 0.18 Tg C yr^{-1} versus 0.25 to 0.5 Tg C yr^{-1}). In the C mass balance (Table 2), it was observed that POC input from the Grijalva River (B6) is high in the RS (64%) but decreases markedly in the DS (2%). The Grijalva River has had substantially reduced TSS flux (~95%) in recent years due to the construction and operation of four dams (Complejo Hidroeléctrico Grijalva) since 1987 [91]. It is probable that POC transport to the Gulf of Mexico had a significant decrease of up to 70% compared with the natural condition proposed by the [16] model. The effects of dams and reservoirs on TSS and POC retention have been studied in several rivers globally [135]. For example, Shi [136] mentions that dams in the Wujiang River, China, have a POC interception rate between 43% and 65%, thus significantly affecting downstream C sources and fluxes. It is also probable that the effect will be more significant if the number of reservoirs in the longitudinal profile of the river is increased [135]. The damming effect in the Grijalva River (B6) is the same as or greater than in other dammed rivers, such as the Nile (Egypt), Rio Grande (USA), Yellow, or Mississippi [91]. The DIC flux in this study was higher than the [16] model but fitted the proposed range (2.44 Tg C yr^{-1} vs. >2 Tg C yr^{-1}).

The C fluxes of the Usumacinta-Grijalva River system are lower than those estimated for large tropical and temperate rivers (e.g., Amazon, Congo, Orinoco, and Mississippi), which is associated with the significantly smaller flow and drainage area of the Usumacinta-Grijalva River basin. Nonetheless, our estimate is comparable to the transport of several tropical (Niger, Zambezi, Godavari, Maroni, and Senegal) and temperate rivers (Danube and Yellow) with similar flows or catchment areas (Table 4).

Table 4. Comparison of the C flux in the Grijalva-Usumacinta system (estimated at the mouth) with the principal rivers of the world. (The Mississippi, Danube, and Yellow rivers are temperate, and the rest are tropical. The area and Q are from [91] data. Flows in parentheses indicate the previous values before the flow reduction due to the construction of reservoirs and irrigation. The C flux for the Tana River is in Gg yr^{-1}, 1 Gg = 10^3 t. 1 Tg = 10^6 t).

River		Area	Q	C Flux (Tg C año^{-1})			Yield (t C km^2 yr^{-1})		
		10^6 (km^2)	(km^3 año^{-1})	DOC	POC	DIC	DOC	POC	DIC
Usumacinta-Grijalva		0.112	120–147	0.29 (0.26–0.33)	0.12 (0.07–0.18)	2.44 (2.29–2.59)	2.61 (2.36–2.99)	1.11 (0.69–1.59)	21.70 (20.4–23.1)
[92]	Amazonas	6.30	6223	26.9	13.2	29.4	5.8	5.5	4.3
[25,93]	Congo	3.80	1300	12.4	2.0	3.5	3.5	0.6	1.0
[26,34]	Orinoco	1.10	1135	5.0	1.7	5.7	4.8	1.6	5.5
[18,99,137]	Mississippi	3.30	570	3.95	2.3	12.25	1.4	2.3	4.2
[52,99,103]	Yellow	0.75	15 (43)	0.06	0.41	1.05	0.1	0.54	1.632
[45]	Irrawaddy	0.43	380 (430)	0.9	2.3–4.3	-	2.2	5.5–10.4	-
[26,77]	Danube	0.79	210.0	0.6	-	7.5	1.2	7.7–12.6	9.6
[26,34,89]	Zambezi	1.31	109.0	0.6	0.5	-	0.1–0.2	0.1	0.7
[99,103]	Niger	1.2	152	0.53	0.66	1.24	0.6	0.5	0.56
[34,94]	Godavari	0.31	92 (120)	0.76	0.28	2.27	-	-	8.0
[97]	Maroni	0.07	63.7	0.34	0.11	-	5.6	1.9	-
[50,77]	Senegal	0.27	24.4	0.1	0.1	-	0.2	0.1	-
[49,51,77]	Tana	0.04	15	11.2	113.3	73.4	0.1	1.4	0.9
[11]	Tropics	63.8	25,123	136.0	131	210.0	2.05	2.13	3.3
[11]	Global	150.0	37,400	215	205	385	1.4	1.3	2.2

DOC and POC fluxes in the Usumacinta-Grijalva River system accounted for just ~7% and ~5.4% of the C flux from the Mississippi River (USA), respectively. However, the Mississippi has a drainage basin ~30 times larger and an annual flow ~five times greater. Despite this, the DOC flux yield of the Usumacinta-Grijalva River system is greater than that calculated by [137] for the Mississippi River (1.72 t C km^2 yr^{-1} versus 1.4 t C km^2 yr^{-1}). The Mississippi POC flux yield is ~twice as high (2.3 t C km^2 yr^{-1} versus 1.1 t C km^2 yr^{-1}) [18] because of the effect of watershed size (Table 4).

The TOC fluxes in the Usumacinta-Grijalva River system (0.35 to 0.49 Tg C yr^{-1}) are lower than that reported for the Zambezi River (1.1 Tg C yr^{-1}; ~109 km^3 yr^{-1}) and Niger River (1.19 Tg C yr^{-1}; ~152 km^3 yr^{-1}). Comparatively, TOC fluxes are similar to the Maroni River (0.4 Tg C yr^{-1}) and slightly higher than the Senegal River (0.2 Tg C yr^{-1}), whose discharges are 63.7 km^3 yr^{-1} and 24.4 km^3 yr^{-1} respectively. Surprisingly, the DOC and POC yield rates from the Usumacinta-Grijalva were higher than in large rivers such as the Yellow, Zambezi, Niger, and Senegal. However, the DOC and POC yield rates of the Maroni River are higher, which can be associated with a smaller drainage area and high forest cover [97].

The Usumacinta-Grijalva River system DIC flux (~2.44 Tg C yr^{-1}) represents one of the highest values of those reported globally (>2 Tg C yr^{-1}) [16]. Thus, this system exports more DIC than the Yellow, Niger, and Godavari and slightly less than the Congo River. The estimated yield (21.7 t C km^2 yr^{-1}) exceeds the large rivers whose drainage area is superior to 400 km^2 (Table 4), such as the Amazon (4.3 t C km^2 yr^{-1}), Congo (1.0 t C km^2 yr^{-1}), Orinoco (5.5 t C km^2 yr^{-1}), and Mississippi (4.2 t C km^2 yr^{-1}).

Only a few DIC yield data similar to this study have been reported, for example in the Brahmaputra River, India-Bangladesh (14.4 t C km^2 yr^{-1}); Xijiang, China (15.38 t C km^2 yr^{-1}); and Pearl, China (13.2 t C km^2 yr^{-1}) [99], as well as in other small monsoon rivers in India, such as the Netravati (17.8 t C km^2 yr^{-1}) and Baitarani (20.7 t C km^2 yr^{-1} [138]. Higher DIC yields have been reported in the tropical mountainous watersheds of western India, such as the Ulhas River (48.5 t C km^2 yr^{-1} [139] or the Kikori River, New Guinea (74.6 t C km^2 yr^{-1}), which has the highest value globally [34]. Therefore, carbonate dissolution is particularly important in the Usumacinta River basin, which exports a higher amount of DIC per unit area than the 25 largest rivers worldwide reported by [99].

Ideally, C concentrations and discharge should be measured simultaneously, at least weekly or monthly, for a robust estimate. The latter would ensure that C export during peak discharge and basal flow would be captured. Therefore, the calculation of the annual

C fluxes is based on: (a) only two dates reflecting the extreme tropical seasonality and (b) the fact that the study year turned out to be wetter than a typical year (i.e., higher flows and higher mass exports of C) and leaves considerable uncertainties. Nonetheless, the obtained data are consistent with those observed in other tropical rivers and with the model reported by [16], and they constitute the urgently needed baseline of the annual C fluxes in the Usumacinta-Grijalva River system.

Moreover, the large spatial scale involved in the present study (~800 km distance to the mouth) and all the variables considered (physicochemical parameters, TSS, Chl-a, and the dissolved and particulate forms of C) provide unique information on the magnitude of the seasonal fluvial contribution in the most important lotic system in Mexico and can be considered a first approximation of the C balances of rivers in the country.

5. Conclusions

This study is the first to estimate the seasonal and spatial variations of the concentrations and export fluxes in DOC, POC, DIC, and PIC in response to hydrologic regimes in the tropical Mexican Usumacinta River during the rainy (2017) and dry (2018) seasons. Seasonal variations played an important role in the C dynamics in the Usumacinta River.

The Pantanos de Centla Biosphere Reserve played a crucial and seasonally variable role in the C fluxes from the Usumacinta River to the Gulf of Mexico. The C balance suggested net retention (C sink) in the floodplains during the rainy season. DOC (~36%), and POC (~9%) fluxes decreased downstream concerning Boca del Cerro (M10). In contrast, in the dry season, the balance showed an increase (C source) of DOC (~5%) and POC (~22%) fluxes. The lower Usumacinta River basin is a sink for DIC in both seasons, with this role being greater in the rainy (~50%) than in the dry (~25%) season. These results are particularly interesting due to changes in riverine C transport and processing concerning the changing climate.

The DOC and POC concentrations showed maximum values during the rainy season, with an increase of approximately two times that during the dry season due to surface erosion and the washing of allochthonous organic matter during the rainfall events. The POC/Chl-a ratios show that organic matter of autochthonous origin can account for a considerable amount of POC during the dry season, mainly in the lower basin. The DOC/POC ratio in both seasons was greater than one, except in the Lacantún River sub-basin, which had a higher POC content during the rainy season. The DOC concentration increases downstream and represents ~66 $\pm$ 17% of the TOC in the rainy season and ~72 $\pm$ 7% of the TOC in the dry season.

The DIC is the most important C fraction in the Usumacinta River, and its concentration is the highest measured for tropical rivers in America. DIC did not present a longitudinal variation but rather remained similar along the mainstem. At most of the sampling sites (except in the Lacantún river sub-basin), the DIC concentration was higher in the dry season, possibly due to a dilution effect in the rainy season and the negative balance of precipitation–evaporation in the dry season.

There is an evident seasonal variation in the C flux into the Gulf of Mexico. The TOC flux during the rainy season was ~15 times higher (~3683 $\pm$ 804 t d^{-1} versus 249 $\pm$ 20 t d^{-1}) and was mainly represented by the dissolved fraction (65% in the rainy season and 75% in the dry season). On the other hand, due to the lithology, the DIC was the main fraction transported to the ocean and was ~4.5 times higher (~14,528 $\pm$ 91 t d^{-1} versus 3228 $\pm$ 224 t d^{-1}) during the rainy season.

The annual C flux for the Usumacinta River is consistent with the Li model [16]. The total carbon flux at the river mouth for the whole Grijalva-Usumacinta River ranged between 2.648 and 3.146 Tg C yr^{-1} (mean 2.879 Tg C yr^{-1}), of which DIC was the most significant fraction transported (85%), followed by DOC (10%), POC (4%), and PIC (<1%). Surprisingly, the estimated yield (21.7 t C km^2 yr^{-1}) of DIC in the Usumacinta-Grijalva River exceeds that of other large rivers such as the Amazon, Congo, Orinoco, and Mississippi.

Supplementary Materials: The following supporting information can be downloaded at: https://www.mdpi.com/article/10.3390/w14172703/s1; Table S1: Sampling sites in the middle and lower basin of the Usumacinta River; Table S2: Summary of the physicochemical variables of the Usumacinta River in the rainy season; Table S3: Summary of the physicochemical variables of the Usumacinta River in the dry season; Table S4: Average values of C ratios (DOC/POC, POC/Chl-a, DIC/DOC) and percentages (DOC/TOC, POC/TSS) in the Usumacinta River during the rainy and the dry seasons; Table S5: C fluxes in the Usumacinta River during the rainy and dry seasons; Figure S1: Discharge variation along the Usumacinta River during the rainy and dry seasons; Figure S2: Chlorophyll-a concentrations along the Usumacinta River during the rainy and dry seasons; Figure S3: Adjustment of the percentage of POC (%) contained in the TSS concerning the TSS concentration of the Usumacinta River in the rainy and dry seasons; Figure S4: Longitudinal variation of the POC/Chl-a ratio with respect to distance from the mouth of the Usumacinta River during the rainy and dry seasons; Figure S5: Longitudinal variation of the DIC/DOC ratio with respect to distance from the mouth of the Usumacinta River during the rainy and dry seasons; Figure S6: PIC adjustment regarding total suspended sediments concentration of the Usumacinta River in the rainy and dry seasons.

Author Contributions: Conceptualization, I.S.-R., J.A., D.C.-L., D.C.-G. and L.A.O.; Data curation, I.S.-R., D.C.-L. and D.C.-G.; Formal analysis, I.S.-R., J.A., S.S.-C., F.G.-O., D.C.-L., D.C.-G. and L.A.O.; Funding acquisition, J.A.; Investigation, I.S.-R., J.A., D.C.-L., D.C.-G. and L.A.O.; Methodology, I.S.-R., J.A., D.C.-L., D.C.-G. and L.A.O.; Project administration, J.A. and L.A.O.; Resources, J.A.; Software, I.S.-R., D.C.-L. and D.C.-G.; Supervision, J.A.; Validation, I.S.-R., J.A., S.S.-C., F.G.-O., D.C.-L., D.C.-G. and L.A.O.; Visualization, I.S.-R., J.A., and L.A.O.; Writing–original draft, I.S.-R., J.A., D.C.-L., D.C.-G. and L.A.O.; Writing–review & editing, I.S.-R., J.A., S.S.-C., F.G.-O., D.C.-L., D.C.-G. and L.A.O. All authors have read and agreed to the published version of the manuscript.

Funding: This research was funded by the FORDECYT-CONACYT Project 273646 "Fortalecimiento de las capacidades científicas y tecnológicas para la gestión territorial sustentable de la Cuenca del Río Usumacinta y su Zona Marina de Influencia (CRUZMI), así como su adaptación ante el cambio climático", the UNAM-PAPIIT Project IN216818 "Flujos de carbono, nutrientes y sedimentos en un sistema lótico tropical", the Programa de Investigación en Cambio Climático, UNAM, Projects PINCC 2020 & PINCC 2021 "Cuerpos acuáticos epicontinentales: papel en la dinámica del carbono y emisiones de gases de efecto invernadero en México", and the Ministerio de Ciencia e Innovación, Consejo Superior de Investigaciones Científicas de España Project COOPA20433 "Contribución del neotrópico acuático continental a las emisiones de gases de efecto invernadero" and COOPA20472 "Los grandes ríos del neotrópico y su contribución al ciclo de carbono global".

Institutional Review Board Statement: Not applicable.

Informed Consent Statement: Not applicable.

Data Availability Statement: The data supporting this study's findings are available from the corresponding author (J.A.) upon reasonable request.

Acknowledgments: We would like to thank the "Posgrado en Ciencias del Mar y Limnología, UNAM", and CONACYT grants awarded to I.S.-R. Also, Ismael Soria-Reinoso received support from the Ecuadorian Secretariat for Higher Education, Science, Technology, and Innovation (SENESCYT, Award No. CZ03-380-2018). Jorge Ramírez and Julio Díaz helped with fieldwork and data collecting. Natura y Ecosistemas Mexicanos AC foundation supported with logistic services at the Chajul Biological Station.

Conflicts of Interest: The authors declare no conflict of interest.

References

1. Battin, T.J.; Luyssaert, S.; Kaplan, L.A.; Aufdenkampe, A.K.; Richter, A.; Tranvik, L.J. The boundless carbon cycle. *Nat. Geosci.* **2009**, *2*, 598–600. [CrossRef]
2. Cole, J.J.; Prairie, Y.T.; Caraco, N.F.; McDowell, W.H.; Tranvik, L.J.; Striegl, R.G.; Duarte, C.M.; Kortelainen, P.; Downing, J.A.; Middelburg, J.J.; et al. Plumbing the global carbon cycle: Integrating inland waters into the terrestrial carbon budget. *Ecosystems* **2007**, *10*, 171–184. [CrossRef]
3. Tranvik, L.J.; Cole, J.J.; Prairie, Y.T. The study of carbon in inland waters-from isolated ecosystems to players in the global carbon cycle. *Limnol. Oceanogr. Lett.* **2018**, *3*, 41–48. [CrossRef]

4. Vachon, D.; Sponseller, R.; Karlsson, J. Integrating carbon emission, accumulation, and transport in inland waters to understand their role in the global carbon cycle. *Glob. Chang. Biol.* **2021**, *27*, 719–727. [CrossRef] [PubMed]
5. Drake, T.W.; Raymond, P.A.; Spencer, R.G.M. Terrestrial carbon inputs to inland waters: A current synthesis of estimates and uncertainty. *Limnol. Oceanogr. Lett.* **2017**, *3*, 132–142. [CrossRef]
6. Bertassoli, D.J.; Sawakuchi, A.O.; Sawakuchi, H.O.; Pupim, F.N.; Hartmann, G.A.; McGlue, M.M.; Chiessi, C.M.; Zabel, M.; Schefuß, E.; Pereira, T.S.; et al. The fate of carbon in sediments of the Xingu and Tapajós clearwater rivers, Eastern Amazon. *Front. Mar. Sci.* **2017**, *4*, 44. [CrossRef]
7. Keller, C.K. Carbon Exports from terrestrial ecosystems: A critical-zone framework. *Ecosystems* **2019**, *22*, 1691–1705. [CrossRef]
8. Raymond, P.A.; Hartmann, J.; Lauerwald, R.; Sobek, S.; McDonald, C.; Hoover, M.; Butman, D.; Striegl, R.; Mayorga, E.; Humborg, C.; et al. Global carbon dioxide emissions from inland waters. *Nature* **2013**, *503*, 355–359. [CrossRef] [PubMed]
9. Li, M.; Peng, C.; Zhang, K.; Xu, L.; Wang, J.; Yang, Y.; Li, P.; Liu, Z.; He, N. Headwater stream ecosystem: An important source of greenhouse gases to the atmosphere. *Water Res.* **2021**, *190*, 116738. [CrossRef]
10. Alvarez-Cobelas, M.; Angeler, D.G.; Sánchez-Carrillo, S.; Almendros, G. A worldwide view of organic carbon export from catchments. *Biogeochemistry* **2012**, *107*, 275–293. [CrossRef]
11. Huang, T.-H.; Fu, Y.-H.; Pan, P.-Y. Fluvial carbon fluxes in tropical rivers. *Curr. Opin. Environ. Sustain.* **2012**, *4*, 162–169. [CrossRef]
12. Meybeck, M. Origins and behaviors of carbon species in world rivers. In *Soil Erosion and Carbon Dynamics*; Roose, E.J., Lal, R., Feller, C., Barthes, B., Stewart, B.A., Eds.; CRC Press.: New York, NY, USA, 2005; pp. 209–238. [CrossRef]
13. Aufdenkampe, A.K.; Mayorga, E.; Raymond, P.A.; Melack, J.M.; Doney, S.C.; Alin, S.R.; Aalto, R.E.; Yoo, K. Rivers and the coupling of biogeochemical cycles. *Front. Ecol. Environ.* **2011**, *9*, 53–60. [CrossRef]
14. Xenopoulos, M.A.; Downing, J.A.; Kumar, M.D.; Menden-Deuer, S.; Voss, M. Headwaters to Oceans: Ecological and Biogeochemical contrasts across the aquatic continuum. *Limnol. Oceanogr.* **2017**, *62*, S3–S14. [CrossRef]
15. Ward, N.D.; Bianchi, T.S.; Medeiros, P.M.; Seidel, M.; Richey, J.E.; Keil, R.G.; Sawakuchi, H.O. Where carbon goes when water flows: Carbon cycling across the Aquatic Continuum. *Front. Mar. Sci.* **2017**, *4*, 7. [CrossRef]
16. Li, M.; Peng, C.; Wang, M.; Xue, W.; Zhang, K.; Wang, K.; Shi, G.; Zhu, Q. The Carbon flux of global rivers: A re-evaluation of amount and spatial patterns. *Ecol. Indic.* **2017**, *80*, 40–51. [CrossRef]
17. Friedlingstein, P.; O'Sullivan, M.; Jones, M.W.; Andrew, R.M.; Hauck, J.; Olsen, A.; Peters, G.P.; Peters, W.; Pongratz, J.; Sitch, S.; et al. Global carbon budget 2020. *Earth Syst. Sci. Data* **2020**, *12*, 3269–3340. [CrossRef]
18. Cai, Y.; Guo, L.; Wang, X.; Aiken, G. Abundance, stable isotopic composition, and export fluxes of DOC, POC, and DIC from the Lower Mississippi River during 2006–2008. *J. Geophys. Res. G Biogeosci.* **2015**, *120*, 2273–2288. [CrossRef]
19. Battin, T.J.; Kaplan, L.A.; Findlay, S.; Hopkinson, C.S.; Marti, E.; Packman, A.I.; Denis Newbold, J.; Sabater, F. Biophysical controls on organic carbon fluxes in fluvial networks. *Prog. Artic. Nat. Geosci.* **2008**, *1*, 95–100. [CrossRef]
20. Schlesinger, W.H.; Bernhardt, E.S. *Biogeochemistry: An Analysis of Global Change*, 4th ed.; Academic Press: Cambridge, MA, USA, 2020.
21. Harrison, J.A.; Caraco, N.; Seitzinger, S.P. Global patterns and sources of Dissolved Organic Matter export to the coastal zone: Results from a spatially explicit, global model. *Glob. Biogeochem. Cycles* **2005**, *19*, GB4S04. [CrossRef]
22. Tian, H.; Yang, Q.; Najjar, R.; Ren, W.; Friedrichs, M.; Hopkinson, C.; Pan, S. Anthropogenic and Climatic Influences on Carbon fluxes from eastern North America to the Atlantic Ocean: A process-based modeling study. *J. Geophys. Res. Biogeosci.* **2015**, *120*, 752–772. [CrossRef]
23. Bouchez, J.; Galy, V.; Hilton, R.G.; Gaillardet, J.; Moreira-Turcq, P.; Pérez, M.A.; France-Lanord, C.; Maurice, L. Source, transport and fluxes of Amazon River particulate organic carbon: Insights from river sediment depth-profiles. *Geochim. Cosmochim. Acta* **2014**, *133*, 280–298. [CrossRef]
24. Schlesinger, W.H.; Melack, J.M. Transport of organic carbon in the world's rivers. *Tellus* **1981**, *33*, 172–187. [CrossRef]
25. Seyler, P.; Coynel, A.; Moreira-Turcq, P.; Etcheber, H.; Colas, C.; Orange, D.; Bricquet, J.P.; Laraque, A.; Guyot, J.; Olivry, J.C.; et al. Organic carbon transported by the equatorial rivers: Example of Congo-Zaire and Amazon Basins. In *Soil Erosion and Carbon Dynamics*; Roose, E.J., Lal, R., Feller, C., Barthes, B., Stewart, B.A., Eds.; CRC Press: Boca Raton, FL, USA, 2005; pp. 255–274. [CrossRef]
26. Ludwig, W.; Probst, J.L. Predicting the oceanic input of organic carbon by continental erosion. *Glob. Biogeochem. Cycles* **1996**, *10*, 23–41. [CrossRef]
27. Galy, V.; Peucker-Ehrenbrink, B.; Eglinton, T. Global carbon export from the terrestrial biosphere controlled by erosion. *Nature* **2015**, *521*, 204–207. [CrossRef]
28. Gaillardet, J.; Calmels, D.; Romero-Mujalli, G.; Zakharova, E.; Hartmann, J. Global climate control on carbonate weathering intensity. *Chem. Geol.* **2018**, *527*, 118762. [CrossRef]
29. Meybeck, M. Global occurrence of major elements in rivers. *Treatise Geochem.* **2003**, *5*, 207–223. [CrossRef]
30. Raymond, P.A.; Hamilton, S.K. Anthropogenic influences on riverine fluxes of Dissolved Inorganic Carbon to the oceans. *Limnol. Oceanogr. Lett.* **2018**, *3*, 143–155. [CrossRef]
31. Raymond, P.A.; Oh, N.; Turner, R.E.; Broussard, W. Anthropogenically enhanced fluxes of water and carbon from the Mississippi River. *Nature* **2008**, *451*, 449–452. [CrossRef]
32. Ludwig, W.; Amiotte-Suchet, P.; Munhoven, G.; Probst, J.L. Atmospheric CO2 consumption by continental erosion: Present-day controls and implications for the last glacial maximum. *Glob. Planet. Chang.* **1998**, *16-17*, 107–120. [CrossRef]

33. Hope, D.; Billett, M.F.; Cresser, M.S. A Review of the export of carbon in river water: Fluxes and processes. *Environ. Pollut.* **1994**, *84*, 301–324. [CrossRef]
34. Gaillardet, J.; Dupré, B.; Louvat, P.; Allègre, C.J. Global silicate weathering and CO_2 consumption rates deduced from the chemistry of large rivers. *Chem. Geol.* **1999**, *159*, 3–30. [CrossRef]
35. Probst, J.L.; Mortatti, J.; Tardy, Y. Carbon river fluxes and weathering CO_2 consumption in the Congo and Amazon River Basins. *Appl. Geochem.* **1994**, *9*, 1–13. [CrossRef]
36. Syvitski, J.; Cohen, S.; Kettner, A.J.; Brakenridge, G.R. How important and different are tropical rivers? —*An overview. Geomorphology* **2014**, *227*, 5–17. [CrossRef]
37. Borges, A.V.; Darchambeau, F.; Teodoru, C.R.; Marwick, T.R.; Tamooh, F.; Geeraert, N.; Omengo, F.O.; Guérin, F.; Lambert, T.; Morana, C.; et al. Globally significant greenhouse-gas emissions from African inland waters. *Nat. Geosci.* **2015**, *8*, 637–642. [CrossRef]
38. Mora, A.; Laraque, A.; Moreira-Turcq, P.; Alfonso, J.A. Temporal variation and fluxes of dissolved and particulate organic carbon in the Apure, Caura and Orinoco Rivers, Venezuela. *J. S. Am. Earth Sci.* **2014**, *54*, 47–56. [CrossRef]
39. Goldsmith, S.T.; Berry Lyons, W.; Harmon, R.S.; Harmon, B.A.; Carey, A.E.; McElwee, G.T.; Berry-Lyons, W.; Harmon, R.S.; Harmon, B.A.; Carey, A.E.; et al. Organic Carbon Concentrations and Transport in Small Mountain Rivers, Panama. *Appl. Geochem.* **2015**, *63*, 540–549. [CrossRef]
40. Seidel, M.; Dittmar, T.; Ward, N.D.; Krusche, A.V.; Richey, J.E.; Yager, P.L.; Medeiros, P.M. Seasonal and Spatial Variability of Dissolved Organic Matter Composition in the Lower Amazon River. *Biogeochemistry* **2016**, *131*, 281–302. [CrossRef]
41. Drake, T.W.; Hemingway, J.D.; Kurek, M.R.; Peucker-Ehrenbrink, B.; Brown, K.A.; Holmes, R.M.; Galy, V.; Moura, J.M.S.; Mitsuya, M.; Wassenaar, L.I.; et al. The Pulse of the Amazon: Fluxes of Dissolved Organic Carbon, Nutrients, and Ions from the World's Largest River. *Glob. Biogeochem. Cycles* **2021**, *35*, e2020GB006895. [CrossRef]
42. Cuevas-Lara, D.; Alcocer, J.; Cortés-Guzmán, D.; Soria-Reinoso, I.F.; García-Oliva, F.; Sánchez-Carrillo, S.; Oseguera, L.A. Particulate Organic Carbon in the Tropical Usumacinta River, southeast Mexico: Concentration, Flux, and Sources. *Water* **2021**, *13*, 1561. [CrossRef]
43. Richey, J.E.; Spencer, R.G.M.; Drake, T.W.; Ward, N.D. Fluvial carbon dynamics across the Land to Ocean Continuum of great tropical rivers: The Amazon and Congo. In *Congo Basin Hydrology, Climate, and Biogeochemistry*; Tshimanga, R.M., N'kaya, G.D.M., Alsdorf, D., Eds.; American Geophysical Union: Washington, DC, USA, 2022; pp. 393–411. [CrossRef]
44. Belliard, J.P.; Hernandez, S.; Temmerman, S.; Suello, R.H.; Dominguez-Granda, L.E.; Rosado-Moncayo, A.M.; Ramos-Veliz, J.A.; Parra-Narera, R.N.; Pollete-Ramirez, K.; Govers, G.; et al. Carbon dynamics and CO_2 and CH_4 exchange in the mangrove dominated Guayas River delta, Ecuador. *Estuar. Coast. Shelf Sci.* **2022**, *267*, 107766. [CrossRef]
45. Bird, M.I.; Robinson, R.A.J.; Oo, N.W.; Aye, M.M.; Lu, X.X.; Higgitt, D.L.; Swe, A.; Tun, T.; Lhaing Win, S.; Sandar Aye, K.; et al. A preliminary estimate of organic carbon transport by the Ayeyarwady (Irrawaddy) and Thanlwin (Salween) Rivers of Myanmar. *Quat. Int.* **2008**, *186*, 113–122. [CrossRef]
46. Bouillon, S.; Yambélé, A.; Spencer, R.G.M.; Gillikin, D.P.; Hernes, P.J.; Six, J.; Merckx, R.; Borges, A.V. Organic matter sources, fluxes and greenhouse gas exchange in the Oubangui River (Congo River Basin). *Biogeosciences* **2012**, *9*, 2045–2062. [CrossRef]
47. Tamooh, F.; Van Den Meersche, K.; Meysman, F.; Marwick, T.R.; Borges, A.V.; Merckx, R.; Dehairs, F.; Schmidt, S.; Nyunja, J.; Bouillon, S. Distribution and origin of suspended matter and organic carbon pools in the Tana River Basin, Kenya. *Biogeosciences* **2012**, *9*, 2905–2920. [CrossRef]
48. Tamooh, F.; Borges, A.V.; Meysman, F.J.R.; Van Den Meersche, K.; Dehairs, F.; Merckx, R.; Bouillon, S. Dynamics of Dissolved Inorganic Carbon and aquatic metabolism in the Tana River Basin, Kenya. *Biogeosciences* **2013**, *10*, 6911–6928. [CrossRef]
49. Tamooh, F.; Meysman, F.J.R.; Borges, A.V.; Marwick, T.R.; Van Den Meersche, K.; Dehairs, F.; Merckx, R.; Bouillon, S. Sediment and carbon fluxes along a longitudinal gradient in the lower Tana River (Kenya). *J. Geophys. Res. G Biogeosci.* **2014**, *119*, 1340–1353. [CrossRef]
50. Mbaye, M.L.; Gaye, A.T.; Spitzy, A.; Dähnke, K.; Afouda, A.; Gaye, B. Seasonal and spatial variation in suspended matter, organic carbon, nitrogen, and nutrient concentrations of the Senegal River in West Africa. *Limnologica* **2016**, *57*, 1–13. [CrossRef]
51. Geeraert, N.; Omengo, F.O.; Tamooh, F.; Marwick, T.R.; Borges, A.V.; Govers, G.; Bouillon, S. Seasonal and inter-annual variations in carbon fluxes in a tropical river system (Tana River, Kenya). *Aquat. Sci.* **2018**, *80*, 19. [CrossRef]
52. Ran, L.; Lu, X.X.; Sun, H.; Han, J.; Li, R.; Zhang, J. Spatial and seasonal variability of Organic Carbon transport in the Yellow River, China. *J. Hydrol.* **2013**, *498*, 76–88. [CrossRef]
53. Krishna, M.S.; Prasad, V.R.; Sarma, V.V.S.S.; Reddy, N.P.C.; Hemalatha, K.P.J.; Rao, Y.V. Fluxes of Dissolved Organic Carbon and nitrogen to the northern Indian Ocean from the Indian monsoonal rivers. *J. Geophys. Res. Biogeosci.* **2015**, *120*, 2067–2080. [CrossRef]
54. Le, T.P.Q.; Phung, T.X.B.; Duong, T.T.; Le, D.; Ho, C.T. Relationship of dissolved inorganic carbon (DIC) concentrations with some Environmental variables in the Red River water in the period 2008–2015. *J. Vietnam. Environ.* **2016**, *8*, 102–106. [CrossRef]
55. Le, T.P.Q.; Dao, V.N.; Rochelle-Newall, E.; Garnier, J.; Lu, X.; Billen, G.; Duong, T.T.; Ho, C.T.; Etcheber, H.; Nguyen, T.M.H.; et al. Total organic carbon fluxes of the Red River System (Vietnam). *Earth Surf. Process. Landf.* **2017**, *42*, 1329–1341. [CrossRef]
56. Huang, T.-H.; Chen, C.-T.A.; Tseng, H.-C.; Lou, J.Y.; Wang, S.L.; Yang, L.; Kandasamy, S.; Gao, X.; Wang, J.T.; Aldrian, E.; et al. Riverine carbon fluxes to the south China Sea. *J. Geophys. Res. Biogeosci.* **2017**, *122*, 1239–1259. [CrossRef]

57. Qin, C.; Li, S.; Yue, F.; Xu, S.; Ding, H. Spatiotemporal variations of dissolved inorganic carbon and controlling factors in a small karstic catchment, southwestern China. *Earth Surf. Process. Landf.* **2019**, *44*, 2423–2436. [CrossRef]
58. Alcocer, J.; Caballero, M.; Ruiz-Fernández, A.C.; Oseguera-Pérez, L.A.; Sánchez-Cabeza, J.A.; Cuevas-Lara, D.; Soria-Reinoso, I. Ecosistemas Acuáticos Epicontinentales. In *Estado del Ciclo del Carbono en México. Agenda Azul y Verde*; Paz Pellat, F., Hernández Ayón, M., Sosa Ávalos, R., Velázquez, A., Eds.; Programa Mexicano del Carbono: Texcoco, Mexico, 2019; p. 716.
59. Butman, D.; Striegl, R.G.; Stackpoole, S.M.; Del Giorgio, P.A.; Prairie, Y.T.; Pilcher, D.; Raymond, P.A.; Paz Pellat, F.; Alcocer, J. Inland Waters. In *Second State of the Carbon Cycle Report (SOCCR2): A Sustained Assessment Report*; Cavallaro, N., Shrestha, G., Birdsey, R., Mayes, M., Najar, R., Reed, S.C., Romero-Lankao, P., Zhu, Z., Eds.; U.S. Global Change Research Program: Washington, DC, USA, 2018; pp. 568–595. [CrossRef]
60. Sánchez-Carrillo, S.; Alcocer, J.; Vargas-Sánchez, M.; Soria-Reinoso, I.; Rivera-Herrera, E.M.; Cortés-Guzmán, D.; Guzmán-Arias, A.P.; Merino-Ibarra, M.; Oseguera-Pérez, L.A. Greenhouse gas emissions from Mexican inland waters: First estimation and uncertainty using an upscaling approach. *Inland Waters* **2022**, *18*, 294–310. [CrossRef]
61. Benke, A.C.; Cushing, C.E. Rivers of North America. In *Encyclopedia of Inland Waters*; Elsevier: Amsterdam, The Netherlands, 2009; pp. 425–437.
62. Alcocer, J.; Bernal-Brooks, F.W. Limnology in Mexico. *Hydrobiologia* **2010**, *644*, 15–68. [CrossRef]
63. Muñoz-Salinas, E.; Castillo, M. Streamflow and sediment load assessment from 1950 to 2006 in the Usumacinta and Grijalva Rivers (Southern Mexico) and the influence of ENSO. *Catena* **2015**, *127*, 270–278. [CrossRef]
64. Lewis, W.; Hamilton, S.; Saunders, J. Rivers of northern South America. In *Ecosystems of the World: Rivers*; Cushing, C.E., Cummins, K.W., Eds.; Elsevier: New York, NY, USA, 1995; Volume III, pp. 219–256.
65. Araujo, M.; Noriega, C.; Lefévre, N. Nutrients and carbon fluxes in the estuaries of major rivers flowing into the tropical Atlantic. *Front. Mar. Sci.* **2014**, *1*, 10. [CrossRef]
66. Bianchi, T.S.; Wysocki, L.A.; Stewart, M.; Filley, T.R.; McKee, B.A. Temporal variability in terrestrially-derived sources of particulate organic carbon in the Lower Mississippi River and its upper tributaries. *Geochim. Cosmochim. Acta* **2007**, *71*, 4425–4437. [CrossRef]
67. Duan, S.; He, Y.; Kaushal, S.S.; Bianchi, T.S. Impact of wetland decline on decreasing dissolved organic carbon concentrations along the Mississippi River continuum. *Front. Mar. Sci.* **2017**, *3*, 280. [CrossRef]
68. Delduco, E.M.; Xu, Y.J. Dissolved carbon transport and processing in north America's largest swamp river entering the northern Gulf of Mexico. *Water* **2019**, *11*, 1395. [CrossRef]
69. Yáñez-Arancibia, A.; Day, J.W. Environmental sub-regions in the Gulf of Mexico coastal zone: The ecosystem approach as an integrated management tool. *Ocean Coast. Manag.* **2004**, *47*, 727–757. [CrossRef]
70. Horton, A.J.; Nygren, A.; Diaz-Perera, M.A.; Kummu, M. Flood severity along the Usumacinta River, Mexico: Identifying the anthropogenic signature of tropical forest conversion. *J. Hydrol. X* **2021**, *10*, 100072. [CrossRef]
71. Muñoz-Salinas, E.; Castillo, M.; Sanderson, D.; Kinnaird, T.; Cruz-Zaragoza, E. Using three different approaches of OSL for the study of young fluvial sediments at the coastal plain of the Usumacinta—Grijalva River basin, Southern Mexico. *Earth Surf. Process. Landf.* **2016**, *41*, 823–834. [CrossRef]
72. Grodsky, S.A.; Carton, J.A. The Intertropical Convergence Zone in the south Atlantic and the equatorial cold tongue. *Am. Meteorol. Soc.* **2003**, *16*, 723–733. [CrossRef]
73. Soares, D.; García, A. *La Cuenca del Río Usumacinta desde la Perspectiva del Cambio Climático*, 1st ed.; Instituto Mexicano de Tecnología del Agua: Jiutepec, México, 2017.
74. Herrera-Silveira, J.A.; Lara-Domínguez, A.L.; Day, J.W.; Yáñez-Arancibia, A.; Ojeda, S.M.; Hernández, C.T.; Kemp, G.P. Ecosystem functioning and sustainable management in coastal systems with high freshwater input in the southern Gulf of Mexico and Yucatan Peninsula. In *Coasts and Estuaries—The Future*; Elsevier Inc.: Amsterdam, The Netherlands, 2019. [CrossRef]
75. Magaña, V.; Vázquez, J.L.; Párez, J.L.; Pérez, J.B. Impact of El Niño on precipitation in Mexico. *Geofís. Int.* **2003**, *42*, 313–330.
76. CONAGUA. Banco Nacional de Datos de Aguas Superficiales (BANDAS). Available online: http://www.conagua.gob.mx/CONAGUA07/Contenido/Documentos/PortadaBANDAS.htm (accessed on 17 May 2021).
77. Meybeck, M.; Ragu, A. GEMS-GLORI World River Discharge Database. Available online: https://doi.pangaea.de/10.1594/PANGAEA.804574 (accessed on 9 March 2022).
78. González-Ramírez, J.; Parés-Sierra, A. Streamflow Modeling of Five Major Rivers That Flow into the Gulf of Mexico Using SWAT. *Atmosfera* **2019**, *32*, 261–272. [CrossRef]
79. March, I.; Castro, M. La cuenca del río Usumacinta: Perfil y perspectivas para su conservación y desarrollo sustentable. In *Las Cuencas Hidrográficas de México: Diagnostico y Priorización*; Cotler-Ávalos, E., Ed.; Pluralia Ediciones e Impresiones: Mexico City, Mexico, 2010; pp. 193–197.
80. Yáñez-Arancibia, A.; Day, J.W.; Currie-Alder, B. Functioning of the Grijalva-Usumacinta River delta, Mexico: Challenges for coastal management. *Ocean. Yearb.* **2009**, *23*, 473–501. [CrossRef]
81. Reyes, E.; Day, J.W.; Lara-Domínguez, A.L.; Sánchez-Gil, P.; Lomelí, D.Z.; Yáñez-Arancibia, A. Assessing coastal management plans using watershed spatial models for the Mississippi delta, USA, and the Usumacinta-Grijalva delta, Mexico. *Ocean Coast. Manag.* **2004**, *47*, 693–708. [CrossRef]

82. Saavedra Guerrero, A.; López López, D.M.; Castellanos Fajardo, L.A. Descripción del medio físico de la cuenca media del Río Usumacinta en México. In *Conservación y Desarrollo Sustentable en la Selva Lacandona. 25 Años de Actividades y Experiencias*; Carabias, J., de La Maza, J., Cadena, R., Eds.; Natura y Ecosistemas Mexicanos A.C.: Mexico City, Mexico, 2015; pp. 19–34.
83. Marshall, J.S. The geomorphology and physiographic provinces of Central America. In *Central America: Geology, Resources, and Hazards*; Bundschuh, J., Alvarado, G.E., Eds.; CRC Press: Boca Raton, FL, USA, 2007.
84. West, R.; Psuty, N.; Thom, B. *Las Tierras Bajas de Tabasco en el Sureste de México*; Gobierno del Estado de Tabasco: Villahermosa, Mexico, 1985; 409p.
85. Olea-Olea, S.; Alcocer, J.; Armienta, M.A.; Oseguera, L.A. Geochemical modeling unravels the water chemical changes along the largest Mexican River. *Appl. Geochem.* **2022**, *137*, 105157. [CrossRef]
86. Arar, E.J.; Collins, G.B. *Method 445.0—In Vitro Determination of Chlorophyll a and Pheophytin a in Marine and Freshwater Algae by Fluorescence*; United States Environmental Protection Agency—Office of Research and Development, National Exposure Research Laboratory: Cincinnati, OH, USA, 1997.
87. Geeraert, N.; Omengo, F.O.; Borges, A.V.; Govers, G.; Bouillon, S. Shifts in the carbon dynamics in a tropical lowland river system (Tana River, Kenya) during flooded and non-flooded conditions. *Biogeochemistry* **2017**, *132*, 141–163. [CrossRef]
88. Meybeck, M. Carbon, nitrogen, and phosphorus transport by world rivers. *Am. J. Sci.* **1982**, *282*, 401–450. [CrossRef]
89. Lambert, T.; Teodoru, C.R.; Nyoni, F.C.; Bouillon, S.; Darchambeau, F.; Massicotte, P.; Borges, A.V. Along-stream transport and transformation of dissolved organic matter in a large tropical river. *Biogeosciences* **2016**, *13*, 2727–2741. [CrossRef]
90. Boeglin, J.-L.; Probst, J.-L.; Nyeck, B.; Ndam-Ngoupayou, J.-R.; Nyeck, B.; Etcheber, H.; Mortatti, J.; Braun, J.-J. Soil carbon stock and river carbon fluxes in humid tropical environments: The Nyong River Basin (South Cameroon). In *Soil Erosion and Carbon Dynamics*; Roose, E.J., Lal, R., Feller, C., Barthès, B., Stewart, B.A., Eds.; CRC Press: Boca Raton, FL, USA, 2005; pp. 275–287. [CrossRef]
91. Milliman, J.D.; Farnsworth, K.L. *River Discharge to the Coastal Ocean: A Global Synthesis*; Cambridge University Press: Cambridge, UK, 2011. [CrossRef]
92. Moreira-Turcq, P.; Seyler, P.; Guyot, J.L.; Etcheber, H. Exportation of organic carbon from the Amazon River and its main tributaries. *Hydrol. Process.* **2003**, *17*, 1329–1344. [CrossRef]
93. Coynel, A.; Seyler, P.; Etcheber, H.; Meybeck, M.; Orange, D. Spatial and seasonal dynamics of total suspended sediment and organic carbon species in the Congo River. *Glob. Biogeochem. Cycles* **2005**, *19*, 1–17. [CrossRef]
94. Balakrishna, K.; Probst, J.L. Organic carbon transport and C/N ratio variations in a large tropical river: Godavari as a case study, India. *Biogeochemistry* **2005**, *73*, 457–473. [CrossRef]
95. Sarin, M.M.; Sudheer, A.K.; Balakrishna, K. Significance of riverine carbon transport: A case study of a large tropical river, Godavari (India). *Sci. China* **2002**, *45*, 97–108.
96. Brunet, F.; Dubois, K.; Veizer, J.; Nkoue Ndondo, G.R.; Ndam Ngoupayou, J.R.; Boeglin, J.L.; Probst, J.L. Terrestrial and fluvial carbon fluxes in a tropical watershed: Nyong basin, Cameroon. *Chem. Geol.* **2009**, *265*, 563–572. [CrossRef]
97. Gallay, M.; Mora, A.; Martinez, J.M.; Gardel, A.; Laraque, A.; Sarrazin, M.; Beaucher, E.; Doudou, J.C.; Lagane, C. Dynamics and fluxes of organic carbon and nitrogen in two Guiana shield river basins impacted by deforestation and mining activities. *Hydrol. Process.* **2018**, *32*, 17–29. [CrossRef]
98. Liu, J.; Song, X.; Wang, Z.; Yang, L.; Sun, Z.; Wang, W. Variations of carbon transport in the Yellow River, China. *Hydrol. Res.* **2015**, *46*, 746–762. [CrossRef]
99. Cai, W.-J.; Dai, M.; Zhang, L.; Guo, X.; Harrison, P.J.; Yin, K.; Zhai, W.; Lohrenz, S.E.; Wang, Y.; Chen, C.-T.A. A Comparative overview of weathering intensity and HCO_3^- flux in the world's major rivers with emphasis on the Changjiang, Huanghe, Zhujiang (Pearl) and Mississippi Rivers. *Cont. Shelf Res.* **2008**, *28*, 1538–1549. [CrossRef]
100. Depetris, P.; Kempe, S. Carbon dynamics and sources in the Parana River. *Limnol. Oceanogr.* **1993**, *38*, 382–395. [CrossRef]
101. Amiotte Suchet, P.; Probst, J.-L.; Ludwig, W. Worldwide distribution of continental rock lithology: Implications for the atmospheric/Soil CO_2 uptake by continental weathering and alkalinity river transport to the oceans. *Glob. Biogeochem. Cycles* **2003**, *17*, 2. [CrossRef]
102. Hélie, J.-F.; Hillaire-Marcel, C.; Rondeau, B. Seasonal changes in the sources and fluxes of dissolved inorganic carbon through the St. Lawrence River—Isotopic and chemical constraint. *Chem. Geol.* **2002**, *186*, 117–138. [CrossRef]
103. Degens, E.; Kempe, S.; Richey, J.E. *SCOPE 42. Biogeochemistry of Major World Rivers Degens*; John Wiley & Sons: New York, NY, USA, 1991.
104. Meybeck, M. Riverine transport of atmospheric carbon: Sources, global typology and budget. *Water Air Soil Pollut.* **1993**, *70*, 443–463. [CrossRef]
105. Bouillon, S.; Abril, G.; Borges, A.V.; Dehairs, F.; Govers, G.; Hughes, H.J.; Merckx, R.; Meysman, F.J.R.; Nyunja, J.; Osburn, C.; et al. Distribution, origin and cycling of carbon in the Tana River (Kenya): A dry season basin-scale survey from headwaters to the delta. *Biogeosciences* **2009**, *6*, 2475–2493. [CrossRef]
106. Cai, Y.; Shim, M.-J.; Guo, L.; Shiller, A. Floodplain influence on carbon speciation and fluxes from the lower Pearl River, Mississippi. *Geochim. Cosmochim. Acta* **2016**, *186*, 189–206. [CrossRef]
107. Aldrian, E.; Chen, T.A.; Adi, S.; Prihartanto; Sudiana, N.; Nugroho, S.P. Spatial and seasonal dynamics of riverine carbon fluxes of the Brantas catchment in East Java. *J. Geophys. Res. Biogeosci.* **2008**, *113*, G3. [CrossRef]

108. Mann, P.J.; Spencer, R.G.M.; Dinga, B.J.; Poulsen, J.R.; Hernes, P.J.; Fiske, G.; Salter, M.E.; Wang, Z.A.; Hoering, K.A.; Six, J.; et al. The biogeochemistry of carbon across a gradient of streams and rivers within the Congo Basin. *J. Geophys. Res. Biogeosci.* **2014**, *119*, 687–702. [CrossRef]
109. Atkins, M.L.; Santos, I.R.; Maher, D.T. Seasonal exports and drivers of dissolved inorganic and organic carbon, carbon dioxide, methane and $\delta^{13}C$ signatures in a subtropical river network. *Sci. Total Environ.* **2017**, *575*, 545–563. [CrossRef]
110. Tweed, S.; Leblanc, M.; Bass, A.; Harrington, G.A.; Munksgaard, N.; Bird, M.I. Leaky savannas: The significance of lateral carbon fluxes in the seasonal tropics. *Hydrol. Process.* **2016**, *30*, 873–887. [CrossRef]
111. Mcclanahan, K.; Polk, J.; Groves, C.; Osterhoudt, L.; Grubbs, S. Dissolved inorganic carbon sourcing using δ ^{13}C-DIC from a karst influenced river system. *Earth Surf. Process Landf.* **2015**, *41*, 392–405. [CrossRef]
112. Hedges, J.I.; Mayorga, E.; Tsamakis, E.; Mcclain, M.E.; Quay, P.; Richey, J.E.; Benner, R.; Opsahl, S.; Black, B.; Quintanilla, J.; et al. Organic matter in Bolivian tributaries of the Amazon River: A comparison to the lower mainstream. *Limnology* **2000**, *45*, 1449–1466. [CrossRef]
113. Dalmagro, H.J.; Johnson, M.S.; de Musis, C.R.; Lathuillière, M.J.; Graesser, J.; Pinto-Júnior, O.B.; Couto, E.G. Spatial patterns of DOC concentration and DOM optical properties in a Brazilian tropical river-wetland system. *J. Geophys. Res. Biogeosci.* **2017**, *122*, 1883–1902. [CrossRef]
114. Rodiles Hernández, R.; González-Díaz, A.A.; González-Acosta, A.F. Ecosistemas acuáticos. In *La Biodiversidad en Chiapas: Estudio de Estado*; CONABIO: Mexico City, Mexico, 2013; pp. 45–57.
115. The Ramsar Convention. Ramsar Sites Information Services. Available online: https://rsis.ramsar.org/es/ris-search/?language=es&f[0]=regionCountry_es_ss%3AGuatemala&pagetab=1 (accessed on 30 May 2019).
116. CONAP. Consejo Nacional de Áreas Protegidas, Guatemala. Available online: http://www.conap.gob.gt/ (accessed on 15 July 2019).
117. SEMARNAT. Secretaría de Medio Ambiente y Recursos Naturales, SEMARNAT. Available online: http://www.paot.org.mx/centro/ine-semarnat/informe02/estadisticas_2000/informe_2000/03_Suelos/3.1_Suelos/index.htm (accessed on 21 July 2019).
118. INEGI. Instituto Nacional de Estadística y Geografía (INEGI). Available online: http://www.inegi.org.mx/ (accessed on 26 November 2018).
119. Thurman, E.M. *Organic Geochemistry of Natural Waters*; Springer Science and Business Media LLC: Denver, CO, USA, 1985. [CrossRef]
120. Abril, G.; Nogueira, M.; Etcheber, H.; Cabeçadas, G.; Lemaire, E.; Brogueira, M.J. Behaviour of organic carbon in nine contrasting European estuaries. *Estuar. Coast. Shelf Sci.* **2002**, *54*, 241–262. [CrossRef]
121. Dudgeon, D. *Tropical Stream Ecology*; Elsevier: Amsterdam, the Netherlands, 2008.
122. Wetzel, R. *Limnology. Lake and River Ecosystem*, 3rd ed.; Academic Press: San Diego, CA, USA, 2001.
123. Wu, Y.; Zhang, J.; Liu, S.M.; Zhang, Z.F.; Yao, Q.Z.; Hong, G.H.; Cooper, L. Sources and distribution of carbon within the Yangtze River system. *Estuar. Coast. Shelf Sci.* **2007**, *71*, 13–25. [CrossRef]
124. Carabias, J.; De la Maza, J.; Cadena, R. Caracterización de la subcuenca del Lacantún. In *Conservación y Desarrollo Sustentable de la Selva Lacandona. 25 Años de Actividades y Experiencias*; Carabias, J., de La Maza, J., Cadena, R., Eds.; Natura y Ecosistemas Mexicanos A.C.: Mexico City, Mexico, 2015; pp. 79–83.
125. Albéric, P.; Pérez, M.A.; Moreira-Turcq, P.; Benedetti, M.F.; Bouillon, S.; Abril, G. Variation of the isotopic composition of dissolved organic carbon during the runoff cycle in the Amazon River and the floodplains. *Comptes Rendus Geosci.* **2018**, *350*, 65–75. [CrossRef]
126. Aucour, A.-M.; Sheppard, S.M.F.; Guyomar, O.; Wattelet, J. Use of ^{13}C to trace origin and cycling of inorganic carbon in the Rhône River System. *Chem. Geol.* **1999**, *159*, 87–105. [CrossRef]
127. Tapia-Silva, F.-O.; Contreras-Silva, A.-I.; Rosales-Arriaga, E.-R. Hydrological characterization of the Usumacinta River basin towards the preservation of environmental services. *Int. Arch. Photogramm. Remote Sens. Spat. Inf. Sci.* **2015**, *40*, 1505. [CrossRef]
128. Estrada Loreto, F.; Barba Macías, E.; Ramos Reyes, R. Cobertura temporal de los humedales en la cuenca el Usumacinta, Balancán, Tabasco, México. *Univ. Cienc.* **2013**, *29*, 141–151.
129. Cruz-Ramírez, A.K.; Salcedo, M.; Sánchez, A.J.; Barba Macías, E.; Mendoza Palacios, J.D. Relationship among physicochemical conditions, chlorophyll-a concentration, and cater level in a tropical river–floodplain system. *Int. J. Environ. Sci. Technol.* **2018**, *16*, 3869–3876. [CrossRef]
130. Castillo, M.M. Suspended sediment, nutrients, and chlorophyll in tropical floodplain lakes with different patterns of hydrological connectivity. *Limnologica* **2020**, *82*, 125767. [CrossRef]
131. Sutfin, N.A.; Wohl, E.E.; Dwire, K.A. Banking Carbon: A review of organic carbon storage and physical factors influencing retention in floodplains and riparian ecosystems. *Earth Surf. Process. Landf.* **2016**, *41*, 38–60. [CrossRef]
132. Sanders, L.; Taffs, K.H.; Stokes, D.J.; Sanders, C.J.; Smoak, J.M.; Enrich-Prast, A.; Macklin, P.A.; Santos, I.R.; Marotta, H. Carbon accumulation in Amazonian floodplain lakes: A significant component of Amazon budgets? *Limnol. Oceanogr. Lett.* **2017**, *2*, 29–35. [CrossRef]
133. Plascencia-Vargas, H.; González-Espinosa, M.; Ramírez-Marcial, N.; Alvarez, D.; Musálem-Castillejos, K. Características físico-bióticas de la cuenca del Río Grijalva. In *Montañas, Pueblos y Aguas. Dimensiones y Realidades de la Cuenca Grijalva*; González-Espinosa, M., Brunel, M.C., Eds.; Ecosur: Campeche, Mexico, 2014; pp. 29–79.

134. Lázaro-Vázquez, A.; Castillo, M.M.; Jarquín-Sánchez, A.; Carrillo, L.; Capps, K.A. Temporal changes in the hydrology and nutrient concentrations of a large tropical river: Anthropogenic influence in the lower Grijalva River, Mexico. *River Res. Appl.* **2018**, *34*, 649–660. [CrossRef]
135. Maavara, T.; Lauerwald, R.; Regnier, P.; Van Cappellen, P. Global perturbation of organic carbon cycling by river damming. *Nat. Commun.* **2017**, *8*, 15347. [CrossRef]
136. Shi, J.; Wang, B.; Wang, F.; Peng, X. Sources and fluxes of particulate organic carbon in the Wujiang cascade reservoirs, southwest China. *Inland Waters* **2018**, *8*, 141–147. [CrossRef]
137. Reiman, J.H.; Xu, Y.J. Dissolved carbon export and CO_2 outgassing from the lower Mississippi River—Implications of future river carbon fluxes. *J. Hydrol.* **2019**, *578*, 124093. [CrossRef]
138. Krishna, M.S.; Viswanadham, R.; Prasad, M.H.K.; Kumari, V.R.; Sarma, V.V.S.S. Export fluxes of dissolved inorganic carbon to the northern Indian Ocean from the Indian monsoonal rivers. *Biogeosciences* **2019**, *16*, 505–519. [CrossRef]
139. Kumar Reddy, S.K.; Gupta, H.; Reddy, D.V. Dissolved inorganic carbon export by mountainous tropical rivers of the western Ghats, India. *Chem. Geol.* **2019**, *530*, 119316. [CrossRef]